Obtaining Temperature Dependence of Cell Membrane Permeability Parameters Using Non-Ideal Thermodynamic Assumptions to Mathematically Model Real Cryopreservation Protocols

by

Faranak Yadegari

A thesis submitted in partial fulfillment of the requirements for the degree of

Master of Science

In

Chemical Engineering

Department of Chemical and Materials Engineering

University of Alberta

© Faranak Yadegari, 2022

Abstract

Cryopreservation is the process of preserving biological matter such as cells, tissues, and organs, at sub-zero temperatures for long-term storage. Cells at low temperatures are susceptible to mechanical damage due to intracellular ice formation and osmotic injuries related to increasing concentration of solutes as the pure water solidifies. Cryobiological damage can be mitigated by controlling the cooling rate and using cryoprotective agents (CPAs). Cell injuries at low temperatures are governed by the transport of water and CPAs across the cell membrane leading to cell volume changes, known as the cell osmotic response. Mathematical modeling of the cell osmotic response to non-isotonic solutions at different temperatures is helpful for optimizing cryopreservation protocols. It has been shown that intra- and extracellular solutions at low temperatures are generally thermodynamically non-ideal. Thus, the changing cell volume under non-ideal thermodynamic assumptions can be modeled using the osmotic virial equation proposed by Elliott et al.[1], and obtaining cell membrane permeabilities to water and CPA, L_P^* and P_S^*, the osmotically inactive fraction of the cell, b^* (the asterisks express that these properties are obtained with non-ideal thermodynamic assumptions), and the second and third osmotic virial coefficients of the grouped intracellular solute B_{gg}, and C_{ggg}. Grouped solute is in fact all the non-permeating intracellular solutes treated as a single solute. The temperature dependence of the cell membrane permeability parameters plays an important role in optimizing a cryopreservation protocol by determining the optimum cooling rate, and the steps for the CPA addition or removal.

In this work, we present a new two-part fitting method to obtain the five cell-type-specific parameters at room temperature and 0 ºC and model the temperature dependence of the permeability parameters using the Arrhenius equation for five cell types, namely, human umbilical vein endothelial cells (HUVECs), H9c2 rat myoblasts, porcine corneal endothelial cells (PCECs),

Jurkat T-lymphocyte cell line, and human cerebral microvascular endothelial cells (hCMECs/D3 cell line). Unlike the previous works in this area, the fitting method in this work is based on both equilibrium and kinetic cell volume data, enabling us to overcome the limitations of previous methods, expand our measurements to lower temperatures, and investigate the temperature dependence of the cell-type-specific properties. The data collected from equilibrium cell volume experiments are used to fit for b^*, B_{gg}, and C_{ggg} . Then, the three measured parameters and the data obtained from the kinetic cell volume experiments are used to fit for the two permeability parameters, L_p^* and P_s^*. We also investigated the possibility that the third osmotic virial coefficient, C_{ggg}, being equal to zero would result in a better fit to the experimental data for different cell types at different temperatures, which has not been investigated in previous studies. Finally, the temperature dependence of L_p^* and P_s^* was modeled using Arrhenius equations and the activation energies related to each permeability parameter, $E_{aL_p^*}$ and $E_{aP_s^*}$ were found.

In the final chapter of this thesis, we use the presented model and the calculated parameters for HUVECs as an example to investigate the impact of the non-ideal thermodynamic model on predicting the changing cell volume during the cryopreservation protocol to show the effectiveness of the proposed mathematical model in having a better understanding of the cell osmotic response and consequently, optimizing the cryopreservation protocol.

Preface

This work, with modifications, is being prepared for submission as: Yadegari, F., Gabler Pizarro, L. A., Marquez-Curtis, L. A, Elliott, J. A. W. “Obtaining Temperature Dependence of Cell Membrane Permeability Parameters Using Non-Ideal Thermodynamic Assumptions to Mathematically Model Real Cryopreservation Protocols.” Marquez-Curtis, L. A prepared the PCEC, Jurkat cell, H9c2 cell, and hCMEC suspensions required for the experiments. Gabler Pizarro, L. transferred her knowledge and method of measuring and analyzing the kinetic cell volume data at room temperature to Yadegari, F. Yadegari, F. prepared the HUVEC suspension, conducted all the kinetic and equilibrium experiments at room temperature and 0 ˚C, performed the data analysis and modeling, and wrote the original draft of this thesis. Elliott, J. A. W. provided the methodology, supervision, and funding for this work as well as reviewing and editing the thesis.

فارسی: این دستاورد را به پدر و مادر عزیزم تقدیم میکنم. از این که به من ایمان دارید و همیشه از من و رویاهایم حمایت می کنید بسیار سپاسگزارم.

English: This achievement is dedicated to my dear parents. Thank you so much for believing in me, and always supporting me and my dreams.

Acknowledgment

I would like to thank my supervisor, Dr. Janet A. W. Elliott, for always supporting and guiding me through my graduate studies. I am so grateful to be able to work under your supervision and learn from you.

To Dr. Leah Marquez-Curtis, thank you for teaching me how to work with the cells and the lab equipment and helping me prepare the cell suspensions for my experiments.

To Laura Gabler Pizarro, thank you for teaching me how to work with the Coulter® counter, and transferring your knowledge about cell volume experiments and data analysis to me to continue the research in this area.

Special thanks to my parents and my dear brother, who have always supported me in my academic journey across the world, even though it is unbearably hard to be apart. None of my achievements would have been possible without you and your continuous support and love.

Table of Contents

List of Tables

List of Figures

Chapter 1. Introduction

1.1. Cryopreservation

Cryopreservation is the process of preserving cells, tissues, and organs at low sub-zero temperatures for long-term storage. This preservation method has become a prevalent way of preserving cells used in medical treatments,[2–7] and genes of rare and endangered species of animals[8,9] or plants[10,11] over the past few decades. Cells and tissues at low temperatures are far from their physiological environment, making them susceptible to various injuries due to intracellular ice formation,[12] increasing concentrations of solutes inside and outside the cells,[13] and dehydration.[14] A successful cryopreservation process relies on maximizing cell viability by minimizing the low-temperature injuries. The early studies of the cryopreservation process showed that high cooling rates in the freezing process increase the probability of intracellular ice formation and consequently, mechanical damage to the cell membrane known as rapid cooling injury.[12,15] When cells are in an aqueous medium that has just started to freeze, there is a chemical potential gradient between intra- and extracellular water, which leads to the intracellular water moving out of the cells to remove the chemical potential differential. With sufficiently slow cooling, the intracellular water has enough time to leave the cell before freezing, depressing the intracellular solution's freezing point to lower temperatures, and consequently, reducing the probability of intracellular ice formation. On the other hand, low cooling rates were reported to prolong the exposure to increasing concentration of solutes leading to osmotic stress and toxicity damage to the cells. Therefore, an intermediate cooling rate known as the 'optimal cooling rate' depending on the cell type was introduced by Mazur et al[15] to have the maximum survival after thaw. The optimal cooling rate being oppositely dependent on the probability of intracellular ice formation

and the increasing concentration of solute is known as 'Mazur's two-factor hypothesis' in cryobiology.

1.2. Cryoprotective agents (CPAs); permeability and toxicity

Cryoprotective agents (CPAs) are widely used to mitigate freezing injuries. CPAs have different mechanisms of protection based on their permeability through the cell membrane. Non-permeating CPAs draw the water out of the cell by increasing the extracellular solution concentration and reduce the likelihood of intracellular ice formation.[16] The protective mechanism of permeating CPAs, on the other hand, is related to their colligative properties. Since these molecules can penetrate the cell membrane, they increase the concentration of both intra- and extracellular solutions, leading to freezing point depression. That means that the intracellular ice formation becomes less probable, and the amount of extracellular ice formation is less at each temperature, resulting in a postponed increase in the concentration of solutes.[16,17] Deciding what CPA to use for a cell type, its concentration, and the temperature and rate of addition and removal is of great importance in the cryopreservation process. Most common permeating cryoprotective agents are toxic to cells at high concentrations and long exposure times.[18] Therefore, for designing a cryopreservation process, there should always be a balance between the permeating CPA toxicity and permeability. CPAs with high permeability for a specific cell type need less time to permeate the cells; thus, the lower exposure time will reduce the risk of the CPAs being lethal to the cells. CPA toxicity and permeability are temperature-dependent.[19] The CPA should be added at a high enough temperature to have the acceptable permeability and at a low enough temperature to reduce major toxicity effects. In addition to the toxicity, CPA addition and removal can create severe osmotic stress on the cells leading to osmotic injuries as a function of volume excursions.[20,21] Osmotic damage is more severe with quick addition or removal of permeating CPAs, especially at

higher temperatures when the cells' hydraulic conductivity and CPA permeability are much larger. Therefore, the temperature, the rate, and the technique of addition or removal of a CPA can be determined by creating a balance between CPA permeability and toxicity, and the cells' osmotic tolerance.

1.3. Mathematical modeling of the cryopreservation process

Cell osmotic response in the cryopreservation process is generally governed by the kinetics of water movement, the transport of the cryoprotective agents across the cell membrane, and their temperature dependence. Therefore, mathematical modeling of the cell volume changes during the cryopreservation process enables us to investigate how different variables can affect the cell osmotic response and optimize cryopreservation protocols. Mathematical models of the cell osmotic response are based on thermodynamic theories that calculate the chemical potential of the solutions inside and outside the cells. Common mathematical models of the cell volume changes during the cryopreservation process are inherently based on ideal thermodynamic theories.[21–26] Meanwhile, several studies have reported that their commonly used model lacks the ability to accurately predict the cells' osmotic behavior, and they needed to modify their models to have the best fit to real cell volume changes.[24,25,27,28] Casula et al. modified their model by investigating and explaining complicated cell membrane biological behavior, including the temporary opening of mechanosensitive channels after being in contact with permeating or non-permeating solutes.[28] One strong explanation for the deviation of common models from real cell behavior is that the solutions inside and outside the cells at cryobiological conditions are generally thermodynamically non-ideal, as they contain multiple solutes at high concentrations. One of the most popular non-ideal thermodynamic theories is the multi-solute form of the osmotic virial equation proposed by Elliott et al. to be used in cryobiology.[1,29] This theory is based on the osmotic virial equation form

of McMillan and Mayer,[30] with a modification that enables the model to consider the interaction between different molecules in the solutions. The osmotic virial coefficients in this model that account for the solution non-ideality are solute specific. Elliott et al.'s form of osmotic virial equation, which is used in this work, requires the exact concentration of every solute in the solutions, which is challenging for a complicated biological system like cytoplasm. In this regard, treating all the non-permeating intracellular solutes as a single 'grouped' solute has been reported to be a valid approach for the osmotic virial equation model.[31] Since different cell types have different cytoplasm compositions, the grouped solute osmotic virial coefficients must be cell-type-specific. Zielinski et al. recently proposed a method of measuring grouped intracellular solute osmotic virial coefficients and used this new method to measure these coefficients for human umbilical vein endothelial cells (HUVECs).[32] Zielinski's work focused on modeling the equilibrium cell volume by exposing the cells to solutions containing permeating and non-permeating CPAs and measuring the second and third osmotic virial coefficients of the grouped solute, B_{gg}, and C_{ggg}, and the osmotically inactive fraction of the cell, b^*. However, in order to model the cell volume during the whole cryopreservation process, the changing cell volume must also be modeled by measuring the cell membrane permeability to water (L_P^*) and CPA (P_S^*). More recently, Gabler Pizarro et al. proposed a new iterative method that uses the kinetic cell volume data resulting from exposing the cells to permeating and non-permeating CPAs to measure the five cell-type-specific parameters: b^*, L_P^*, P_S^*, B_{gg}, and C_{ggg}, and modelled the kinetic cell volume data for HUVECs and H9c2 cells.[33] Gabler Pizarro et al.'s method is based on kinetic volume data that does not necessarily reach the equilibrium state, which confines this method's applicability to room temperature. One difficulty for Gabler Pizarro in measuring these parameters at 0 ºC was the long time required for the cells to reach the equilibrium state, which made it impossible to collect the

required kinetic data all the way to the equilibrium in a single run with the Coulter®counter and Cell Size Analyzer program used.[34] Another difficulty encountered by Gabler Pizarro was maintaining a stable enough 0 ºC temperature throughout the long measurement time needed.[34]

1.3. Cells of interest in this work

The experimental kinetic and equilibrium cell volume data in this work was collected for five different cell types: human umbilical vein endothelial cells (HUVECs), H9c2 rat myoblasts, porcine corneal endothelial cells (PCECs), the Jurkat T-lymphocyte cell line, and a human cerebral microvascular endothelial cell line (hCMECs/D3) by exposing them to hypertonic solutions with and without a permeating solute. The chosen cells have different biological properties and functions, and optimizing the cryopreservation process for each of them is very important for clinical and research purposes. Designing an optimized cryopreservation protocol for human umbilical vein endothelial cells (HUVECs) is of great importance because they are a model system for endothelial and vascular biology research and are frequently used in tissue engineering and drug delivery studies.[35–38] H9c2 cells are original skeletal muscle cells derived from embryonic BD_1X rat heart tissue by Kimes and Brandt,[39] which are often used in in vitro studies because of the resemblance of their morphological parameters to immature embryonic cardiomyocytes and their ability to beat.[40–42] Porcine corneal endothelial cell (PCEC) cryopreservation studies have gained lots of attention due to the increasing need for donor corneas worldwide and the renewed interest in the possibility of using corneas from other species, like pigs, that have similar properties to the human cornea for partial thickness keratoplasty or the transplantation of engineered corneal tissue created through endothelial cell expansion as alternative treatments for corneal endothelial disorders.[43–46] Jurkat cells are an immortalized line of human T lymphocytes, first derived from the peripheral blood of a 14-year-old boy suffering from T-cell leukemia.[47] Because Jurkat cells

can simulate the function of T lymphocytes, they are frequently used in in vitro studies of T cell signal transduction, cytokines, and receptor expression, and can provide reference in cell therapy, cancer treatment, blood research, and studies of differentiation, apoptosis, and cell survival.[48–50] Thus, developing an efficient cryopreservation process facilitates the storage and use of these cells for research and clinical applications. The human cerebral microvascular endothelial cell (hCMEC)/D3 line[51] is widely used in in vitro models of the human blood–brain barrier for drug delivery studies.[52,53] The blood–brain barrier regulates the passage of ions, molecules, and cells between the blood vessels lined mainly with continuous endothelial cells and the brain.[54] Optimization of the hCMEC cryopreservation process is of great importance for blood–brain barrier research.[55]

1.4. Scope of this thesis

In this work, I build on Zielinski et al.'s and Gabler Pizarro et al.'s works and introduce an advanced method based on both equilibrium and kinetic cell volume data to calculate the five cell-type-specific parameters, which enables us to expand the measurements to lower temperatures and investigate the temperature dependence of these parameters. The five cell-type-specific parameters are obtained by conducting eight sets of experiments in which the cell suspensions are exposed to a hypertonic solution in the presence and absence of a permeating cryoprotectant, dimethyl sulfoxide (Me_2SO), at equilibrium and kinetic cell volume conditions separately at room temperature and 0 ºC. The hypertonic solutions used in this work are 5x PBS and 3 molal Me_2SO solutions. The data collected from equilibrium cell volume experiments are used to obtain b^*, B_{gg}, and C_{ggg} in an iterative process. The iterative process starts with ideal and dilute assumptions ($B_{gg} = C_{ggg} = 0$) to fit the non-permeating CPA data (5x PBS) and obtain an initial value for b^*. The calculated b^* is used to fit the permeating CPA data (3 molal Me_2SO) and calculate B_{gg} and

C_{ggg}. Then, the calculated B_{gg} and C_{ggg} are used to refit the equilibrium non-permeating CPA data to obtain a new b^*. This iterative process continues until the values of b^*, B_{gg} and C_{ggg} stay the same after an iteration. Then, these three measured parameters and the data from the kinetic cell volume experiments are used to obtain the two other parameters, L_p^* and P_s^* (the asterisks express that these properties are obtained with non-ideal thermodynamic assumptions), from the non-permeating and permeating CPA data, respectively. Thus, in this work, I present a robust method of obtaining the cell-type-specific parameters from specific parts of the cell volume data which have the most information about those parameters, which enables me to overcome the limitations of the previous works and expand the measurements to 0 ºC. I also introduced an efficient method of maintaining a stable enough 0 ºC temperature throughout the long 0 ºC experimental runs in contrast to the previous work by Gabler Pizarro[34]. Furthermore, I investigated the possibility of having a better fit to the experimental cell volume data by assuming that the third osmotic virial coefficient, C_{ggg}, was equal to zero at different temperatures. That assumption means that the second osmotic virial coefficient, B_{gg}, alone, is sufficient to describe the intracellular solution's non-ideality. Finally, the temperature dependence of the permeability parameters is modeled using Arrhenius equations and the activations energies related to each permeability parameter, $E_{aL_p^*}$ and $E_{aP_s^*}$ are calculated. The experiments and the fitting method were conducted for five different cell types, from endothelial cells to lymphocytes and muscle cells, namely, i) human umbilical vein endothelial cells (HUVECs), ii) porcine corneal endothelial cells (PCECs), iii) human cerebral microvascular endothelial cells (hCMEC/D3 cell line), iv) Jurkat T-lymphocyte cell line, and v) H9c2 rat myoblasts.

In the end, I use the calculated parameters in this work to model the cell volume changes during a proposed HUVEC cryopreservation protocol using the ideal and non-ideal thermodynamic

assumptions to show how the presented mathematical model can help cryobiologists better understand the cell osmotic response and why the non-ideal thermodynamic assumptions are important in optimizing cryopreservation protocols. The effects of CPA loading time, cooling rate, and CPA dilution temperature on the cell volume changes during the cryopreservation process are also investigated with ideal and non-ideal thermodynamic assumptions.

Chapter 2. Methodology

In this work, the five cell-type-specific parameters needed for modeling the cell volume changes during a cryopreservation process based on non-ideal thermodynamic assumptions, b^*, L_P^*, P_S^*, B_{gg}, and C_{ggg}, are obtained by using a new two-part, equilibrium and kinetic, curve fitting method. The cell volume data are collected by conducting two sets of experiments in which the cell suspensions are exposed to a hypertonic solution containing sodium chloride (NaCl) in the presence and absence of a permeating cryoprotectant, dimethyl sulfoxide (Me_2SO). In each set of experiments, the kinetic and equilibrium cell volume data after contact with a hypertonic solution are collected separately at room temperature and 0 ºC. The hypertonic solutions used in this work are 5x PBS and 3 molal Me_2SO solutions. The data collected from equilibrium cell volume experiments are used to fit for b^*, B_{gg}, and C_{ggg} using an iterative process. Then, the three measured parameters obtained from the equilibrium part and the data obtained from the kinetic cell volume experiments are used to fit for the two permeability parameters, L_p^* and P_s^*. The details of the experiments and the fitting method are explained thoroughly in this chapter.

2.1. Experimental methods

2.1.1. Cell preparations

Human umbilical vein endothelial cells (HUVECs, Lonza, Walkersville, MD, USA) were kept frozen in a liquid nitrogen Dewar as pooled primary cells until needed. For each set of experiments, a vial of frozen HUVECs was rapidly thawed in a 37 ºC water bath and then diluted in 5 mL of Endothelial Basal Medium-2 (EBM-2) (Lonza, Walkersville, MD, USA) that was supplemented with Endothelial Cell Growth Medium-2 Bulletkit (EGM-2, Lonza), consisting of ascorbic acid, fetal bovine serum (FBS), hydrocortisone, R3 insulin-like growth factor (R3-IGF-1), human fibroblast growth factor B (hFGF-B), vascular endothelial growth factor (VEGF), and

human endothelial growth factor (hEGF). Then, the cells were sub-cultured in 75 cm^2 tissue culture flasks with 15 mL of the complete medium in an incubator at 37 ºC and 5% CO_2. After reaching 70–90% confluence, the cells were passaged using 0.025% trypsin/0.01% EDTA (Lonza). Then, they were centrifuged at 1000 rpm for 5 minutes at room temperature in an Eppendorf 5810R tabletop centrifuge (Eppendorf AG, Hamburg, Germany). After that, the supernatant was removed, the cell count and isotonic size were determined using a Coulter® Z2™ particle count and size analyzer (Beckman Coulter, Mississauga, ON, Canada). The cell count was used to calculate the amount of medium needed to prepare the desired cell concentration for the experiments, and the cell size was used to determine which control bead size and aperture to use for volume measurements.

Leah Marquez-Curtis prepared the primary porcine corneal endothelial cell (PCEC) suspensions needed for the experiments. The methods were as previously described[44], with some modifications. Pig eyeballs were obtained through a local meat market (Kim Fat Market Ltd., Edmonton, AB) from pigs freshly slaughtered for meat processing. They were transported to the laboratory in a Styrofoam box with a cooled gel pack designed to protect the samples from freezing or over-heating. Upon arrival in the lab, the eyeballs were wrapped in gauze soaked in chlortetracycline antibiotic (50 mg/mL, Sigma-Aldrich, Oakville, ON, Canada), left for 15 min, and then transferred to a designated biosafety cabinet. The cornea was excised from the eyeball using sterile scalpel and surgical scissors along with 1 to 2 mm of surrounding scleral tissue, and placed in a sterile 24-well tissue culture plate with the endothelial side up. The cornea was rinsed with Ca^{2+}- and Mg^{2+}-free phosphate buffered saline (PBS, Gibco Life Technologies, Grand Island, NY, USA), and then treated with TrypLE Express Enzyme (1X, Gibco), and incubated for 10 min at 37 ºC. The dislodged cells were aspirated with a sterile pipette tip and centrifuged at 600 g for

2 min. The cell pellet was resuspended in Dulbecco's Modified Eagle Medium (DMEM, Gibco) supplemented with 4.5 mg/mL glucose, 4 mM L-glutamine, 10% FBS, and 1% antibiotic-antimycotic agent (10,000 units/mL of penicillin, 10,000 mg/mL of streptomycin, and 25 mg/mL of amphotericin B, Gibco), and then seeded in tissue culture flasks and incubated at 37 °C. The medium was changed every 2–3 days until a confluent cell monolayer was formed. The cells were detached by treating with TrypLE Express and incubating at 37 °C for 10–12 min centrifuged at 500 g for 5 min. After that, the supernatant was removed, the cell count and isotonic size were determined using a Coulter® Z2™ particle count and size analyzer (Beckman Coulter). The cell count was used to calculate the amount of medium needed to prepare the desired cell concentration for the experiments, and the cell size was used to determine which control bead size and aperture to use for volume measurements.

Leah Marquez-Curtis prepared the H9c2 suspensions needed for the experiments. Briefly, the methods were as follows: H9c2(2-1) (ATCC® CRL1446™, Manassas, VA, USA) cell line was received in dry ice cryopreserved in complete growth medium supplemented with 5% (v/v) dimethyl sulfoxide and was kept in a liquid nitrogen storage Dewar until use. Frozen cells were thawed rapidly in a 37 °C water bath. DMEM (ATCC 30-2002) supplemented with 10% fetal bovine serum (Gibco) was added, and cells were plated in T75 tissue culture flasks (Corning 430641, Millipore Sigma, Burlington, MA, USA). They were incubated in a humidified CO_2 (5%) incubator at 37 °C, and medium change was carried out every 2–3 days. When the cells were 50–70% confluent, they were passaged by trypsinization using 0.25% trypsin/0.53 mM EDTA solution (Gibco). Cells in suspension were centrifuged at 140 g for 6 min, the supernatant was removed, and the cell pellet was resuspended in fresh complete medium. The cell count and isotonic size were determined using a Coulter® Z2™ particle count and size analyzer (Beckman Coulter). The

cell count was used to calculate the amount of medium needed to prepare the desired cell concentration for the experiments, and the cell size was used to determine which control bead size and aperture to use for volume measurements.

Leah Marquez-Curtis prepared the human cerebral microvascular endothelial cell suspensions needed for the experiments. The methods were as previously described.[55] Human cerebral microvascular endothelial cell/D3 line (hCMEC/D3 cell line, CLU512, Cedarlane, CELLutions Biosystems Inc., Burlington, ON, Canada) was kept in a liquid nitrogen storage Dewar upon receipt. Frozen cells were retrieved from liquid nitrogen and thawed rapidly in a 37 °C water bath. The culture medium consisting of endothelial basal medium (EBM, Lonza), 5% FBS (Gibco, 10270-106), 1% chemically defined lipid concentrate (Life Technologies, 111905031), 1.4 μM hydrocortisone (Millipore Sigma, H0135), 5 μg/mL ascorbic acid (A4544, Millipore Sigma), 1% penicillin/streptomycin (Life Technologies), 10 mM HEPES (Life Technologies, 15630–080) and 1 ng/mL basic fibroblast growth factor (Millipore Sigma, F0291), was added. The cells were plated on Falcon flasks (Thermo Fisher Scientific, Ottawa, ON, Canada) pre-coated with Cultrex rat collagen I (Trevigen, R&D Systems, Minneapolis, MN, USA). The flasks were incubated in a humidified CO_2 (5%) incubator at 37 °C. After reaching about 80% confluence, the cells were passaged using 0.25% trypsin-EDTA solution (Gibco, Thermo Fisher Scientific), and incubation at 37˚C for 3 minutes. EBM complete medium (with FBS and the other supplements described above) was then added to inactivate trypsin, and centrifugation was carried out at 1000 g for 10 minutes in an Eppendorf 5810R tabletop centrifuge (Eppendorf AG, Hamburg, Germany). The cell count and isotonic size were determined using a Coulter® Z2™ particle count and size analyzer (Beckman Coulter). The cell count was used to calculate the amount of medium needed to prepare the desired cell concentration for the experiments, and the cell size was used to

determine which control bead size and aperture to use for volume measurements. After the first passage, the cells were sub-cultured in antibiotic-free complete medium.

Leah Marquez-Curtis prepared the Jurkat cell suspensions needed for the experiments. The methods were as follows: Jurkat clone E6-1 line (ATCC® TIB-152™) cells were kept frozen in liquid nitrogen vapor phase until needed. The frozen cells were thawed by gentle agitation in a 37 ºC water bath, then were transferred into a centrifuge tube containing 9 ml of the complete culture medium consisting of RPMI Medium1640 (Gibco, 22400-089) supplemented with 10% fetal bovine serum (FBS, Gibco, Life Technologies). The cell suspension was centrifuged at 1000 rpm for 6 minutes. The cell pellet was resuspended with the culture medium and plated at 1.0–2.5 × 10^5/mL in untreated non-adherent tissue culture flasks. The cells were passaged after 2 days by centrifugation at 1000 rpm for 6 min. The cell count and isotonic size were determined using a Coulter® Z2™ particle count and size analyzer (Beckman Coulter). The cell count was used to calculate the amount of medium needed to prepare the desired cell concentration for the experiments, and the cell size was used to determine the size of the control bead and aperture for volume measurements.

2.1.2. Solution preparations

For each set of experiments, three different solutions were prepared. A stock solution of ten-times phosphate-buffered saline (10x DPBS, Life Technologies, Grand Island, NY, USA) was diluted with deionized water to create the solutions of 1x PBS and 5x PBS. The PBS solutions were prepared by measuring the appropriate volume of each component and mixing them. Then, their exact osmolalities were measured by a Micro-Osmette Model 5004 freezing point depression osmometer (Precision Systems, Inc., Natick, MA, USA). The osmolality of the 10x PBS solution is approximately 3000 mOsm/kg. It was diluted two times to prepare the 5x PBS solution with an

osmolality of 1500 ± 50 mOsm/kg, and ten times to prepare the 1x PBS solution with an osmolality of 300 ± 30 mOsm/kg to be used in cell isotonic volume measurements. A 3 molal dimethyl sulfoxide solution (Me_2SO, Sigma-Aldrich, Oakville, ON, Canada) was prepared using the prepared 1x PBS solution as solvent. 500 g of 1x PBS solution and 117.195 g of pure Me_2SO were weighed using a Mettler Toledo PG603-S analytical balance (Mettler Toledo, Mississauga, ON, Canada) and mixed to make the 3 molal Me_2SO solution.

2.1.3. Determining cell viability

The experiments and the fitting method in this work are designed based on the assumption that the majority of the cells are alive and undamaged during the whole experiment. Therefore, the viabilities of the cells that had been in contact with the hypertonic solutions with or without a permeating CPA were measured using trypan blue viability assessment. Trypan blue assay is a stain exclusion assessment that stains dead cells with compromised cell membranes blue and leaves membrane-intact cells unstained. 30 μm^3 of the cell suspensions were mixed 1:14 with the 5x PBS and three molal Me_2SOs solutions separately, and the mixtures were left as long as a complete experimental run, depending on the hypertonic solution, to equilibrate. The 5x PBS cell suspension was diluted 1:5 in the isotonic solution after the experimental test period. Then, the resulting suspensions were mixed 1:1 with trypan blue solution (trypan blue 0.4%, 0.85% NaCl, Lonza, Walkersville, MD USA), and the live cells were immediately counted on a hemocytometer. Negative controls consisted of cells suddenly plunged into liquid nitrogen and thawed at room temperature, which were almost all dead.

2.1.4. Coulter® ZB1™ Counter

The equilibrium and kinetic cell volumes were measured with a Coulter® ZB1™ Counter (Beckman Coulter, Mississauga, ON, Canada) fitted with a microcomputer interface designed by Dr. Locksley McGann[56] called the Cell Size Analyzer. A Coulter® counter is an electronic particle counter that records a peak value and timestamp of each passing cell through a small aperture on the tube placed inside the experimental solution. The peak value is an expression of the potential displacement across the aperture, varying between 0 and 256 depending on the settings chosen on the Coulter® counter. Adjustable settings, which are the amplification, the aperture current, the matching switch, the gain trim, and the aperture size, were chosen to capture the largest number of peaks measured in an isotonic environment run in the middle of the peak value range depending on the cell type. The aperture size was determined based on the diameter of the cells measured earlier during the cell preparation process; the 100 μm-diameter aperture was used for HUVECs, PCECs, H9c2 cells, and hCMECs, and the 50 μm-diameter aperture was used for Jurkat cells. The aperture current and the maximum switch were set to 1 and 20×10^3, respectively, for all the cell types. For HUVECs, PCECs, and hCMECs, the amplification and gain trim were set to 8 and 9, respectively. For H9c2 cells, the amplification and gain trim were set to 8 and 4, respectively. For Jurkat cells, the amplification and gain trim were set to 32 and 4, respectively. Finally, to calibrate the settings with the measured peak values, three calibration runs were done on each day of experiments with each solution using latex beads (Beckman Coulter, Mississauga, ON, Canada). The size of the latex beads was chosen based on the diameter of the cells. For HUVECs, PCECs, H9c2 cells, and hCMECs, the 15 μm diameter beads were used and for Jurkat cells, the 10 μm diameter beads were used. Then, a calibration factor (f) was calculated based on the average peak value of the calibration runs as $f = \frac{V_{beads}}{p}$, where V_{beads} is the volume of the beads, and p is the

average peak value measured during the calibration run. This factor was used to convert the measured peaks in the runs done with the cells to a value in terms of volume.

2.1.5. Isotonic runs

Isotonic runs were done on each day of experiments to measure the isotonic volume of the cells. Each isotonic run was done by adding 10 ml of the 1x PBS prepared solution to a 20 ml blood dilution vial (VWR International, Edmonton, AB, Canada) and then adding the cell suspension containing 250,000 cells to the vial to reach a concentration of 25,000 cells per milliliter of the cells. This concentration had previously been found to be the best concentration of the cells to capture the rapid shrinkage or swelling of the cells and reduce the risk of clogging the aperture.[33] In order to have a uniform distribution of the cells in the experimental solutions, a stirring magnet was added to the vial, and the vial was placed on an RT Basic Series Stirrer (Thermo Fisher Scientific, Burlington, ON, Canada). The tube of the Coulter® counter, including the aperture, was submerged in the solution. Then, the stirrer was turned on, the Coulter® counter valve was opened, and the Cell Size Analyzer (CSA) data acquisition program was started to record the measured peak values and their timestamps for about 60 seconds. After the run, the CSA program was paused, the Coulter® counter valve was closed, and the mixer was turned off. All the isotonic runs were repeated three times on each day of experiments, and the average of the three data sets was used to calculate the cells' isotonic volume.

2.1.6. Kinetic runs

In the kinetic cell volume experimental runs, the whole volume changing process from the beginning when the cells start to shrink must be covered. Therefore, in the kinetic runs, the cells were added to the vial using a small-tip pipet after the Coulter® counter valve was opened and the Cell Size Analyzer program was set to record the measurements. When the cells were added to the

vial containing 5x PBS, which had a higher osmolality, they shrunk until they reached the final equilibrium volume. When the cells were added to the vial containing 3 molal Me_2SO, they initially shrunk because of the exposure to a hypertonic environment and then swelled back up as the Me_2SO entered the cell and equilibrated between the intra- and extracellular environment. For all the cell types at room temperature, kinetic runs in 5x PBS and 3 molal Me_2SO were continued for 60 seconds and 3 minutes, respectively, to collect enough data on the cell volume changes, except for the Me_2SO runs for the Jurkat cells that were continued for 4 minutes. The kinetic runs at 0 ºC were done for longer times since the shrinkage and swelling for all the cell types are much slower compared to room temperature. For all the cell types, the 5x PBS and 3 molal Me_2SO runs were continued for 2.5 and 3.5 minutes, respectively, to collect enough data on the cell volume changes at 0 ºC, except for the Me_2SO runs for the Jurkat cells that were continued for 5 minutes. All the kinetic runs were repeated three times on each day of experiments to calculate the error bars. Thanks to the new fitting method employed in this work, reaching the equilibrium in the kinetic runs is unnecessary since the equilibrium data were gathered in a separate set of experiments described in the next section.

2.1.7. Equilibrium runs

The time to reach the equilibrium, especially for the 3 molal Me_2SO runs, could be so long that the solution level in the vials would lower and go below the aperture level. This will be even more challenging for low-temperature experiments that require much longer times for the cells to reach equilibrium. To address this problem, a new fitting method that requires gathering the equilibrium cell volume data in separate runs is used in this work. For the equilibrium runs, the time at which the cells reach the equilibrium must be determined in advance. For all the cell types at room temperature, a 2-minute-long set of raw data was collected when the cells were added in

5x PBS runs. For 3 molal Me_2SO runs, on the other hand, the process was longer and more complex. The cell volume data was collected from 3 to 6 minutes after adding the cells to the solution in one run; in another run, the data was collected from 5 to 8 minutes after adding the cells to the solution; and in the last run, the data was collected from 7 to 10 minutes after adding the cells to the solution. At 0 ºC for all the cell types, a 3-minute-long set of raw data was collected when the cells were added in 5x PBS runs. For 3 molal Me_2SO runs, the cell volume data was collected from 7 to 10 minutes after adding the cells to the solution in one run; in another run, the data was collected from 9 to 12 minutes after adding the cells to the solution; and in the last run, the data was collected from 11 to 14 minutes after adding the cells to the solution. The only exception was the 3 molal Me_2SO runs for Jurkat cells at 0 ºC in which the set of runs was done from 15 to 18 minutes, 17 to 20 minutes, and 19 to 22 minutes after adding the cells because it took them much longer to swell back up at 0 ºC. The collected data for these two solutions were statistically analyzed, as explained in section 2.2.3, to determine the time required to reach equilibrium as the time after which the cell volume does not change anymore. After determining the equilibrium time, the equilibrium data was collected by doing the measurements for 30 seconds after the cells had reached equilibrium. The average of the collected data was used as the unique equilibrium cell volume for that run. All the experimental equilibrium runs were repeated three times to calculate the error bars.

2.1.8. Temperature conditions

Several techniques were used to keep the temperature constant during the runs, which was more challenging for 0º C experiments. Meanwhile, in order to consider even the slightest changes in the temperature, the temperature was measured with a Temp300 JTEK Data Logging Thermocouple (Thermo-Fisher Scientific, Singapore) before and after each run, and the average

was used as the run temperature for the data analysis. For room temperature experiments, the environment as an infinite volume compared to the solutions kept the temperature constant. The only disruptive factor was the heat produced by the Coulter® counter lens lamp, which was covered to isolate its heat source. For the 0 ºC experiments, on the other hand, the following steps were performed to keep the temperature constant: First, all the prepared solutions and the cell suspensions were placed in a bucket of ice and water mixture for more than one hour to equilibrate as indicated in Figure 1.a. The Coulter® counter's flushing solutions were also kept in a beaker containing ice and water during the whole experiment. The vials of solutions for each run were covered by a jacket of ice and water mixture (Figure 1.b) during the entire run to avoid any temperature changes while the Coulter® counter was working. The Coulter® counter's lens lamp was covered during the runs, as showed in Figure 1.c.

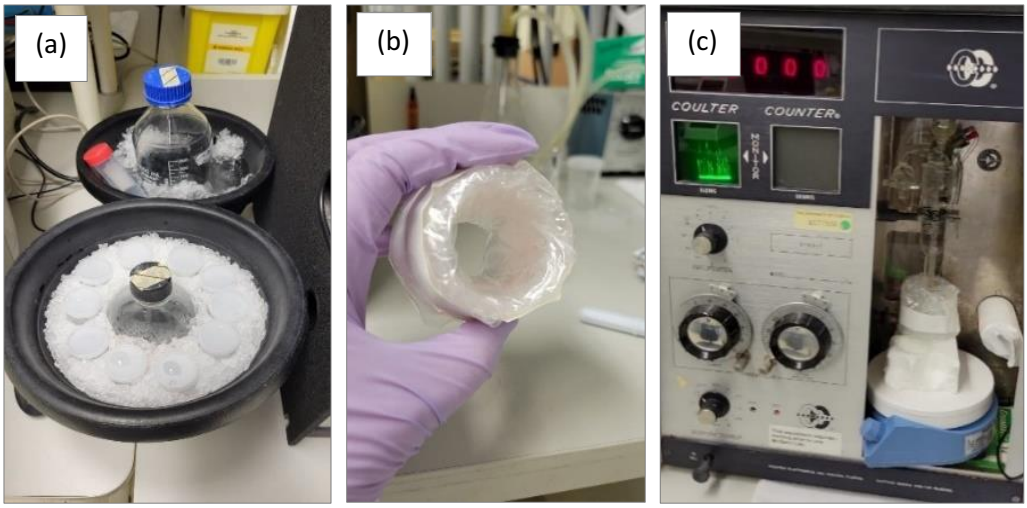

Figure 1. Photographs of the 0 ºC experimental setups showing (a) Solution bottles and vials and the cell suspension in the buckets of the ice–water mixture, (b) Jacket of the ice–water mixture that covers the vials during the runs, and (c) The Coulter® counter during the run.

2.2. Data analysis methods and modeling

In this work, all the cell volume data used to do the equilibrium analysis and the kinetic fittings are the relative cell volume data, which is defined as $\frac{V_{data}}{V_0}$. In this definition, V_{data} is the calculated cell volume using the cell volume outputs of the Coulter® counter and the calibration factors, and V_0 is the measured isotonic cell volume on each day of the experiment.

2.2.1. Cell Size Analyzer program

The data files generated as the output of the Coulter® counter were analyzed by the Cell Size Analyzer (CSA) program created by Dr. Locksley McGann. This program opens a file in one main window (Figure 2) and three additional windows named "Histogram", "Raw Data", and "Mean vs Time". The "Histogram" window, which is indicated in Figure 3 with a 5x PBS run as the sample, shows the peak value distribution or the number of times a peak value within each peak value interval was obtained in the run. The "Raw Data" window shows all the measured peak values versus time, and the "Mean vs Time" window illustrates the mean peak value per assigned time interval versus time, as indicated in Figures 4 and 5, respectively, for the same 5x PBS run. The time interval can be adjusted in the main window, making the mean data versus time less scattered, which is set at 500 milliseconds in this work. The beginning and the end times of the runs can be adjusted by dragging the vertical red lines in the "Raw Data" and checking data "Invalid" for the part that is excluded. Also, the lower and upper thresholds shown as the horizontal red lines in the "Raw Data" window are adjusted with the vertical red lines in the "Histogram" window, or the "Upper" and "Lower" buttons in the main window, to exclude noise.

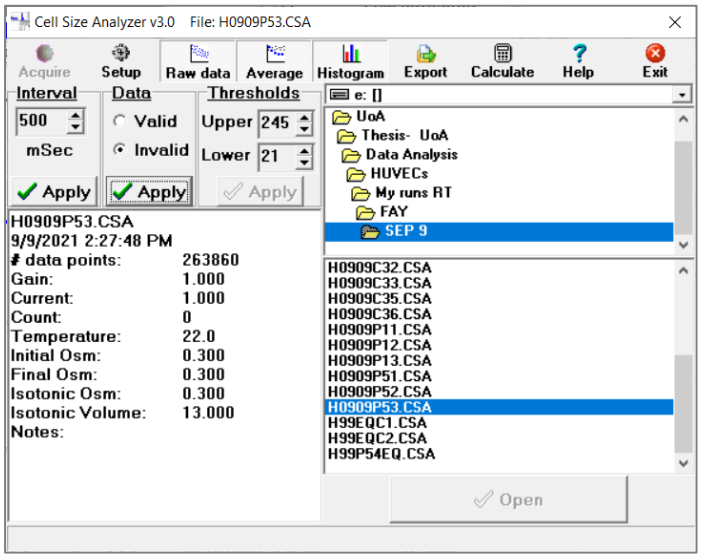

Figure 2. The main window of the CSA program, showing the files generated as Coulter® counter output.

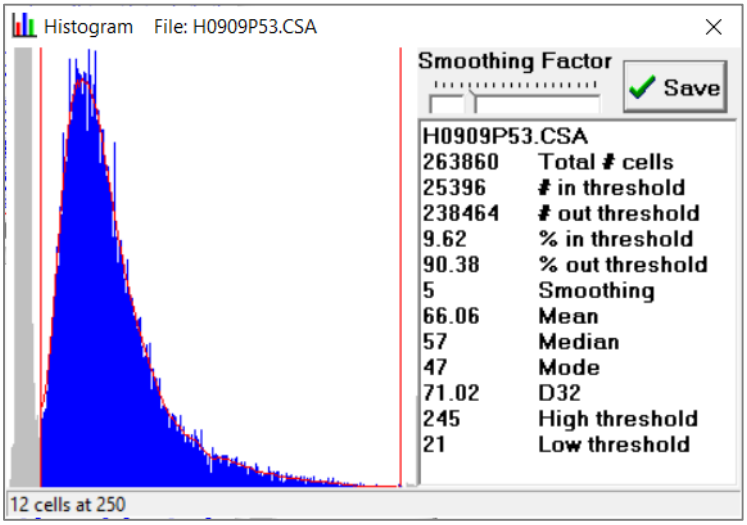

Figure 3. The "Histogram" window of the CSA program displaying the number of cells measured at different peak heights and additional information about the total number of cells, the threshold peak values, the cells within the current threshold, and the average peak value.

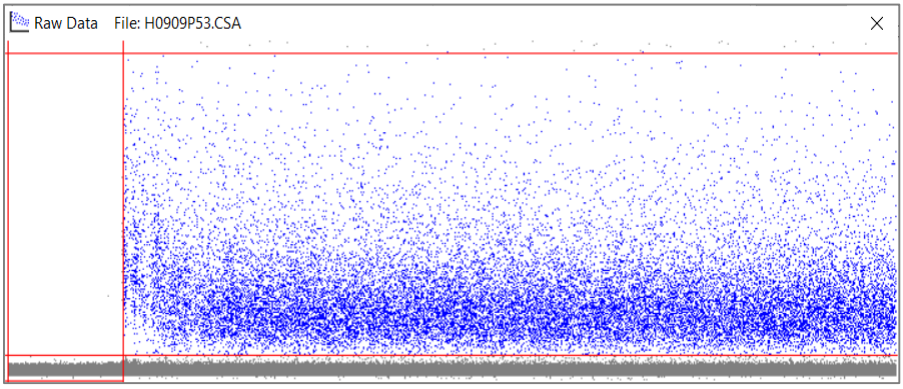

Figure 4. The "Raw Data" window of the CSA program displaying all the measured peak values of data points versus time. The vertical red lines are used to cut out the time span of the data where there are no peaks or the aperture was clogged.

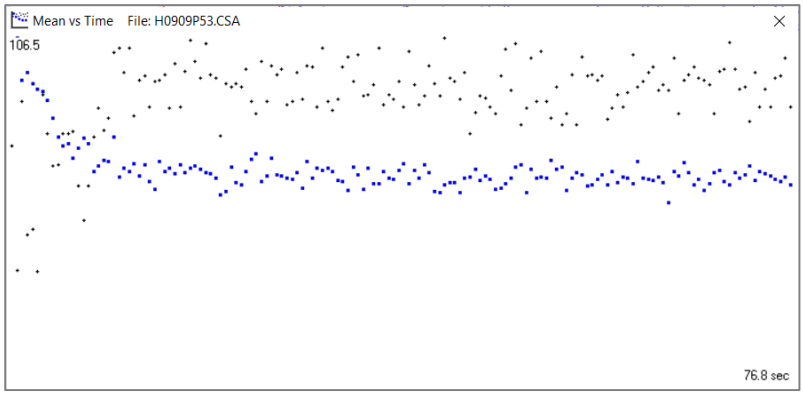

Figure 5. The "Mean vs Time" window of the CSA program, displaying the mean peak measured within the time interval as blue dots and the total number of points per time interval as black dots.

For the isotonic and calibration runs, after conducting the adjustments above, the text that appears in the "Histogram" window is used. The kinetic and equilibrium runs are obtained by adjusting the mentioned settings and clicking on "Export" in the main window, then "Mean vs Time". This process creates a text file with the same information as in the "Histogram" window and the time, the number of peaks per time interval, and the mean peak value in three separate columns. The text files were inserted into Excel, and columns were added to convert the peak values into volume using the calibration factor. Finally, the cell volume was converted into the relative volume by dividing by the measured isotonic volume on the day of experiments.

2.2.2. Equilibrium cell volume model (as published in reference [32])

In this work, the equilibrium cell volume is modeled using the equations from a previous study to obtain the cell-type-specific grouped intracellular solute osmotic virial coefficients and osmotically inactive fraction by curve-fitting the model to experimental measurements. Then, the obtained grouped solute osmotic virial coefficients and osmotically inactive fraction are used to model the kinetic cell volume data to obtain the cell membrane permeability parameters.

The equilibrium cell volume can be generally modeled by the following equations:[32,57]

$$\frac{V_{cell}}{V_{cell}^0} = (1 - b^*)\frac{m_g^0}{m_g^{in}} + \frac{V_p^{in}}{V_{cell}^0} + b^* \quad (1)$$

$$m_p^{in} M_p \rho_1 \left(\frac{V_{cell}}{V_{cell}^0} - b^* - \frac{V_p^{in}}{V_{cell}^0}\right) = \rho_p \frac{V_p^{in}}{V_{cell}^0} \quad (2)$$

$$\pi^{in} = \pi^{ex} \quad (3)$$

and,

$$\mu_p^{in} = \mu_p^{ex} \quad (4)$$

where m_g^{in} is the combined molality of all non-permeating intracellular solutes known as the grouped solute, m_g^0 is the combined molality of all non-permeating intracellular solutes under isotonic conditions (in moles of grouped solute g/kg of water), b^* is the osmotically inactive fraction of the cell, or the volume fraction of the cell contents that cannot leave the cell, V_{cell}^0 is the equilibrium cell volume under isotonic conditions (in μm^3), m_p^{in} is the intracellular molality of permeating solute p (in moles of solute p/kg of water), V_p^{in} is the intracellular volume of solute p (in μm^3), M_p is the molar mass of solute p (in kg/mole), ρ_p is the density of permeating solute p (in kg/ μm^3), ρ_1 is the density of water (in kg/μm^3), V_{cell} is the equilibrium cell volume (in μm^3), π^{in} and π^{ex} are the intra- and extracellular solutions osmolalities (in osmoles/kg of water), and

μ_p^{in} and μ_p^{ex} are the chemical potential of permeating solute p in intra- and extracellular solutions, respectively (in J/mole).

The solutions osmolalities and the permeating solute chemical potential are calculated using the Elliott et al. form of osmotic virial equation as below:[1,29]

$$\pi = \sum_{i=2}^{r} k_i m_i + \sum_{i=2}^{r}\sum_{j=2}^{r}[\frac{(B_{ii}+B_{jj})}{2} k_i m_i k_j m_j] + \sum_{i=2}^{r}\sum_{j=2}^{r}\sum_{k=2}^{r}[(C_{iii}C_{jjj}C_{kkk})^{1/3} k_i m_i k_j m_j k_k m_k] \quad (5)$$

and,[31]

$$\mu_p = k_p\theta_p + RTk_p[\ln(M_1 m_p + \sum_{i=2}^{r}[(B_{ii}+B_{pp})k_i m_i] + \frac{3}{2}\sum_{i=2}^{r}\sum_{j=2}^{r}[(C_{iii}C_{jjj}C_{ppp})^{1/3} k_i m_i k_j m_j]] \quad (6)$$

where m_i is the molality of solute i (in moles of solute i/kg of water), B_{ii} and C_{iii} are the second and third osmotic virial coefficients of solute i, respectively (in [moles of solute i/kg of water]$^{-1}$ and [moles of solute i/kg of water]$^{-2}$, respectively), k_i is the empirical dissociation constant of solute i, R is the universal gas constant (in J/[mole K]), T is the absolute temperature (in K), M_1 is the molar mass of water (in kg/mole), θ_p is a function of temperature and pressure for solute p (in J/mole), and $(r-1)$ is the number of solutes in the solution.

In this work, one permeating cryoprotectant, Me_2SO (p), and one non-permeating solute, NaCl (N), are available in the extracellular solution for permeating CPA runs. The intracellular solution contains the permeating cryoprotectant and all the native compounds of the cells, defined as a grouped solute (g). Thus, based on Equation 5 and 6, Equation 3 becomes:[32]

$$m_p^{in} + m_g^{in} + B_{pp}(m_p^{in})^2 + B_{gg}(m_g^{in})^2 + (B_{pp}+B_{gg})\, m_p^{in} m_g^{in} + C_{ppp}(m_p^{in})^3 +$$

$$3(C_{ppp}^2 C_{ggg})^{1/3}(m_p^{in})^2 m_g^{in} + 3\,(C_{ppp}C_{ggg}^2)^{1/3} m_p^{in}(m_g^{in})^2 + C_{ggg}(m_g^{in})^3 =$$

$$m_p^{ex} + k_N m_N^{ex} + B_{pp}(m_p^{ex})^2 + B_{\mathrm{NN}}(k_N m_N^{ex})^2 + (B_{pp}+B_{\mathrm{NN}})\, m_p^{ex} k_N m_N^{ex} + C_{ppp}(m_p^{ex})^3 +$$

$$3(C_{ppp}^2 C_{\mathrm{NNN}})^{1/3}(m_p^{in})^2 \mathrm{k_N} m_N^{ex} + 3(C_{ppp}C_{NNN}^2)^{1/3} m_p^{ex}(k_N m_N^{ex})^2 + C_{\mathrm{NNN}}(k_N m_N^{ex})^3 \quad (7)$$

and Equation 4 becomes:[32]

$$ln(M_w m_p^{in}) + (B_{pp}+B_{gg})\; m_g^{in} + 3/2(C_{ggg}^2 C_{ppp})^{1/3}\,(m_g^{in})^2 =$$

$$ln(M_w m_p^{ex}) + (B_{pp}+B_{NN})\mathrm{k_N} m_N^{ex} + 3/2(C_{NNN}^2 C_{ppp})^{1/3}(k_N m_N^{ex})^2 \quad (8)$$

where m_g^{in} is the intracellular molality of the grouped solute (g), B_{gg} and C_{ggg} are the second and third osmotic virial coefficients of the grouped solute, respectively (in [moles of grouped solute g/kg of water]$^{-1}$ and [moles of grouped solute g/kg of water]$^{-2}$, respectively), m_N^{ex} is the extracellular molality of NaCl, B_{NN} and C_{NNN} are the second and third osmotic virial coefficients of NaCl, respectively (in [moles of NaCl/kg of water]$^{-1}$ and [moles of NaCl/kg of water]$^{-2}$, respectively), k_N is the dissociation constant of NaCl, and B_{pp} and C_{ppp} are the second and third osmotic virial coefficients of the permeating cryoprotectant (Me_2SO in this case), respectively (in [moles of Me_2SO/kg of water]$^{-1}$ and [moles of Me_2SO/kg of water]$^{-2}$, respectively).

On the other hand, for non-permeating CPA runs, there is only one non-permeating solute present in the extracellular solution, which is NaCl. The intracellular solution also only contains the grouped solute. Therefore, for non-permeating CPA runs Equations 2 and 4 are not needed, and Equation 1 becomes:[32]

$$\frac{V_{cell}}{V_{cell}^0} = (1 - b^*)\,\frac{m_g^0}{m_g^{in}} + b^* \quad (9)$$

And based on Equation 5, Equation 3 becomes: [32]

$$m_g^{in} + B_{gg}\,(m_g^{in})^2 + C_{ggg}\,(m_g^{in})^3 = \pi^{ex} \quad (10)$$

where π^{ex} is measured experimentally.

The water and cryoprotectant densities are assumed to be temperature dependent by the following equations:[58]

$$\rho_w = 999.974950 \times 10^{-18}\left[1 - \frac{(T - 3.983035)^2(T + 301.797)}{522528.9(T + 6934881)}\right] \quad (11)$$

and,[59]

$$\rho_p = -9.87181 \times 10^{-19}T + 1.11979 \times 10^{-15} \quad (12)$$

where ρ_w and ρ_p are the densities of water and the cryoprotectant in kg/μm^3, and T is the temperature of the solution in ℃. The equations used for the equilibrium permeating and non-permeating CPA data fittings are summarized in Table 1 and Table 2, respectively.

Table 1. Equations for modeling the equilibrium permeating CPA data

Equilibrium **permeating CPA equations**[32,58,60]	
$\frac{V_{cell}}{V_{cell}^0} = (1 - b^*)\frac{m_g^0}{m_g^{in}} + \frac{V_p^{in}}{V_{cell}^0} + b^*$	(1)
$m_p^{in} M_p \rho_1 \left(\frac{V_{cell}}{V_{cell}^0} - b^* - \frac{V_p^{in}}{V_{cell}^0}\right) = \rho_p \frac{V_p^{in}}{V_{cell}^0}$	(2)

$$m_p^{in} + m_g^{in} + B_{pp}(m_p^{in})^2 + B_{gg}(m_g^{in})^2 + (B_{pp}+B_{gg})\, m_p^{in} m_g^{in} + C_{ppp}(m_p^{in})^3 + 3(C_{ppp}^2 C_{ggg})^{1/3}(m_p^{in})^2 m_g^{in} + 3\,(C_{ppp} C_{ggg}^2)^{1/3} m_p^{in}(m_g^{in})^2 + C_{ggg}(m_g^{in})^3 = m_p^{ex} + k_N m_N^{ex} + B_{pp}(m_p^{ex})^2 + B_{\mathrm{NN}}(k_N m_N^{ex})^2 + (B_{pp}+B_{NN})\, m_p^{ex} k_N m_N^{ex} + C_{ppp}(m_p^{ex})^3 + 3(C_{ppp}^2 C_{NNN})^{1/3}(m_p^{in})^2 \mathrm{k_N} m_N^{ex} + 3(C_{ppp} C_{NNN}^2)^{1/3} m_p^{ex}(k_N m_N^{ex})^2 + C_{\mathrm{NNN}}(k_N m_N^{ex})^3$$ (7)
$$ln(M_w m_p^{in}) + (B_{pp}+B_{gg})\; m_g^{in} + 3/2(C_{ggg}^2 C_{ppp})^{1/3}\,(m_g^{in})^2 = ln(M_w m_p^{ex}) + (B_{pp}+B_{NN})\mathrm{k_N} m_N^{ex} + 3/2(C_{NNN}^2 C_{ppp})^{1/3}(k_N m_N^{ex})^2$$ (8)
$$\rho_w = 999.974950 \times 10^{-18}\left[1 - \frac{(T-3.983035)^2(T+301.797)}{522528.9(T+6934881)}\right]$$ (11)[58]
$$\rho_p = -9.87181 \times 10^{-19} T + 1.11979 \times 10^{-15}$$ (12)[60]

Table 2. Equations for modeling the equilibrium non-permeating CPA data

Equilibrium **non-permeating CPA equations**[32,57,58]
$$\frac{V_{cell}}{V_{cell}^0} = (1 - b^*)\,\frac{m_g^0}{m_g^{in}} + b^*$$ (9)
$$\pi^{ex} = m_g^{in} + B_{gg}\,(m_g^{in})^2 + C_{ggg}\,(m_g^{in})^3$$ (10)
$$\rho_w = 999.974950 \times 10^{-18}\left[1 - \frac{(T-3.983035)^2(T+301.797)}{522528.9(T+6934881)}\right]$$ (11)[58]

2.2.3. Finding the time of equilibrium

Gathering the equilibrium data in this work is based on statistical proof of the time required by the cells to reach equilibrium. The experimental cell volume data were collected in different time intervals as explained in section 2.1.7. After equilibrium, the cell volume remains constant

over time. Based on this fact, a trend line is fitted to the cell volume data in each 3-minute experimental time interval. The time interval that has a trend line with the closest slope to zero is divided into 30 seconds intervals to find their trend line slopes by the same process. The half-minute interval with the trend line slope smaller than the others and less than 0.01 indicates the interval that the equilibrium begins. To make sure that the specified time interval is the accurate time of equilibrium, several time intervals starting at the equilibrium time with random lengths are fitted to a line to show that their slopes are either equal to or smaller than the slope of the equilibrium interval. Representative graphs of applying this part off the method for HUVECs in permeating CPA runs at room temperature are shown in Figure 6. The absolute slope values in this method can be sensitive to the scatter of the cell volume data. Therefore, for this part of the analysis, the output cell volume data from the Cell Size Analyzer program can be taken at longer time intervals than 500 ms to make the equilibrium slope values slightly closer to zero, which is more expected.

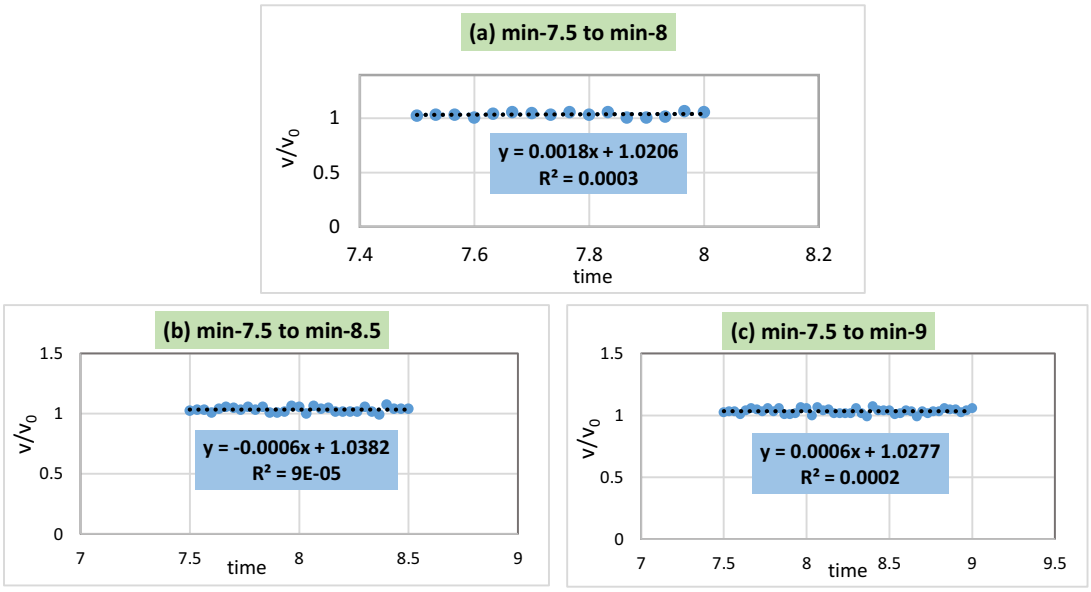

Figure 6. The relative cell volume data and their trend lines for the (a) 30 seconds, (b) 1 minute, and (c) 1.5 minute after equilibrium for a HUVEC Me_2SO run at room temperature.

2.2.4. Equilibrium fitting method

A previous study reported that B_{gg}, and C_{ggg} are more sensitive to cell volume data in the presence of cryoprotectants.[32] Thus, the equilibrium permeating CPA data are fitted with the equations summarized in Table (1) to calculate B_{gg}, and C_{ggg}, and the equilibrium non-permeating CPA data are fitted to the equations in Table (2) to obtain b^*. Therefore, an iterative process is needed here. Starting with ideal and dilute assumptions (B_{gg}= C_{ggg}= 0) and fitting the non-permeating CPA data to the equations in Table (2), an initial value for b^* is obtained. Then the calculated b^* is used to fit the permeating CPA data with the equations in Table (1) to calculate B_{gg}, and C_{ggg}. Then, the newly calculated B_{gg} and C_{ggg} are used to refit the equilibrium non-permeating CPA data to equations in Table (2) to obtain a new b^*. This iterative process continues until the values of b^*, B_{gg}, and C_{ggg} stay the same after an iteration. A flowchart of the equilibrium fitting method is given in Figure 7. To extend the investigations on the grouped solute behavior in terms of the osmotic virial coefficients and the intracellular osmolality, two possible sets of values for B_{gg} and C_{ggg} are also analyzed separately in this work to find the option with the best fit to the experimental cell volume data. The first possible answer is that a three-degree polynomial best describes the grouped solute behavior, meaning both B_{gg} and C_{ggg} have non-zero values. The second possibility assumes that a two-degree polynomial produces the best interpretation of the grouped solute role in intracellular osmolality, meaning C_{ggg} is equal to zero, and B_{gg} is the only osmotic virial coefficient applicable.

The average of all the repeats of cell volume data at equilibrium was given to MATLAB as the unique equilibrium cell volume value. A program was written to solve Equation 9 for b^* using the non-permeating CPA equilibrium volume and the ideal and dilute assumption (B_{gg}= C_{ggg}= 0) as

the initial guess. Subsequently, a program was written to solve Equations 1 and 2 for B_{gg}, and C_{ggg} using the permeating CPA equilibrium volume and the obtained b^* from the first code. In the first program, the built-in nonlinear system solving function "fsolve" from MATLAB was used to solve Equation 10 for m_g^0 and m_g^{in} by providing the initial guesses for these parameters. The experimentally measured values of the extracellular osmolality at isotonic and hypertonic conditions (π^0 and π^{ex}) were given to the code as known parameters. Then, the same function was used to solve for b^* by having m_g^0, m_g^{in}, and the equilibrium volume data. In the second program, a nested loop is utilized to assign certain values with specified ranges and resolutions to B_{gg}, and C_{ggg}. The ranges were set to wide enough intervals to include the values reported for B_{gg}, and C_{ggg} in previous studies. Then, a function named 'root2d' was defined as a system of the two Equations 7 and 8, with the two unknowns m_p^{in} and m_g^{in} , and the function "fsolve" was used to solve this system of equations for m_p^{in} and m_g^{in}. Next, Equations 1 and 2 were solved for the equilibrium cell volume value. Finally, a conditional loop was defined to end the nested loop and introduce the best values for B_{gg}, and C_{ggg}, once the difference between experimental and calculated cell volume at equilibrium was less than a certain threshold. The thresholds are the closest numbers to zero that enable the program to find at least one set of answers for B_{gg}, and C_{ggg}. The obtained B_{gg} and C_{ggg} were used in the first program to obtain a new b^* and continue the iteration. Analyzing the possibility of having a better fit by considering a two-degree polynomial for the grouped solute behavior, meaning $C_{ggg} = 0$, caused some slight changes in the codes, making them more straightforward. In both codes, the value for C_{ggg} was set to zero without exception, and in the second code, the nested loop turned into a simple loop that assigned changeable values to B_{gg} only. The steps of the iterative process of the equilibrium fitting method

until convergence for all the cell types at room temperature and 0 ºC, are illustrated in the Appendix, Table A1 to A10. This iterative fitting method was done for each repeat of the 5x PBS and 3 molal Me_2SO equilibrium runs to calculate the standard deviations for the fitting parameters b^*, B_{gg} and C_{ggg}. The equilibrium iterative fittings used to obtain the standard deviations related to the repeats of H9c2 cells at 0 ºC are reported in the Appendix, Tables A11 to A16, as an example.

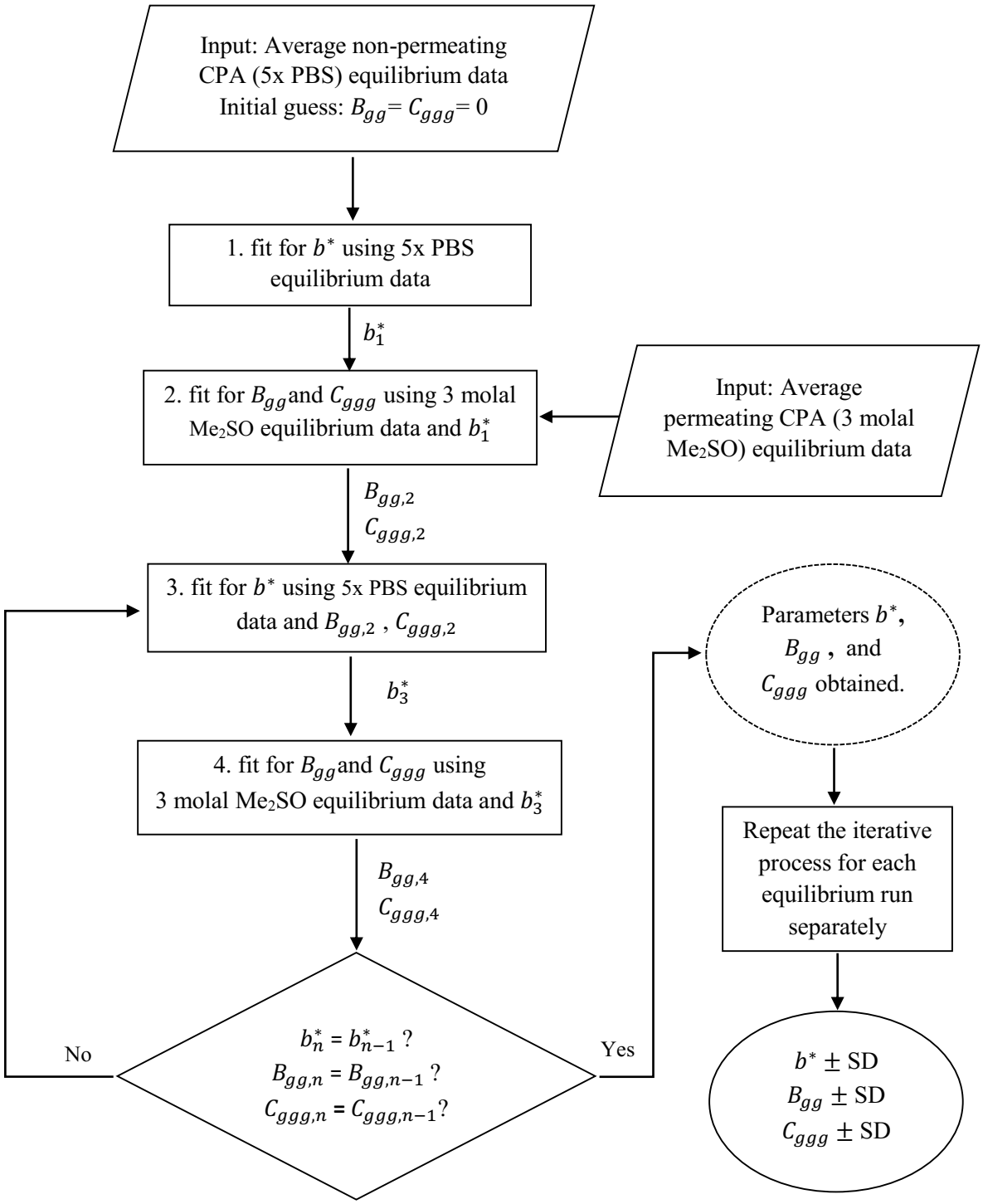

Figure 7. Flowchart of the equilibrium fitting method for obtaining b^* , B_{gg} , C_{ggg}.

2.2.5. Kinetic cell volume model (as published in reference [33])

The cell volume changes before reaching the equilibrium result from water and cryoprotectant transport across the cell membrane which can be generally modeled by the following equations:[32,33,61]

$$\frac{dV_w^{in}}{dt} = L_p^* A_{cell}(t) RT \rho_w [\pi^{in}(t) - \pi^{ex}] \quad (13)$$

$$\frac{dV_p^{in}}{dt} = P_s^* A_{cell}(t) [a_p^{ex} - a_p^{in}(t)] \quad (14)$$

where V_w^{in} and V_p^{in} are the volume of water and volume of cryoprotectant inside the cell, respectively (both in μm^3), L_p^* is the hydraulic conductivity (in μm atm^{-1} min^{-1}), P_s^* is the membrane permeability to permeating solutes or cryoprotectants (in μm min^{-1}), R is the universal gas constant, T is the temperature (in K), ρ_w is the density of water (in kg μm^{-3}), A_{cell} is the surface area of the cell (in μm^2), π^{in} and π^{ex} are the intra- and extracellular osmolalities (in osmoles/kg of water), respectively, and a_p^{in} and a_p^{ex} are the intra- and extracellular activity of the cryoprotectant, respectively. The extracellular solution is assumed to be an infinite solution with constant properties. Therefore, π^{ex} and a_p^{ex} are constant with time. On the other hand, the intracellular osmolality and activity, π^{in} and a_p^{in}, are assumed to change with volume over time.

In addition, L_p^* and P_s^* are assumed to be temperature-dependent with an Arrhenius behavior and are described as:

$$L_P^* = L_p^{*RT} \exp\left[\frac{E_{aL_p^*}}{R}\left(\frac{1}{T_{RT}} - \frac{1}{T}\right)\right] \quad (15)$$

$$P_S^* = P_s^{*RT} \exp\left[\frac{E_{aP_s^*}}{R}\left(\frac{1}{T_{RT}} - \frac{1}{T}\right)\right] \quad (16)$$

where L_p^{*RT} and P_s^{*RT} are the reference points of L_p^* and P_s^* which are measured at room temperature, T_{RT}, and $E_{aL_p^*}$ and $E_{aP_s^*}$ are respective activation energies.

A_{cell}, the surface area of the cell (in μm^2), changes with the volume. Assuming the cells are spherical we will have:

$$A_{cell}(t) = 4\pi \left[\frac{3}{4\pi} V_{cell}(t)\right]^{2/3} \quad (17)$$

where $V_{cell}(t)$ is the total cell volume which is changing with time and is calculated as:

$$V_{cell}(t) = V_w^{in}(t) + V_p^{in}(t) + b^* V_{cell}^0 \quad (18)$$

The activity of the cryoprotectant can be described as:[31,32]

$$a_p = \exp[k_p[\ln(M_1 m_p) + \sum_{i=2}^{r}\left[\left(B_{ii} + B_{pp}\right)k_i m_i\right] + \frac{3}{2}\sum_{i=2}^{r}\sum_{j=2}^{r}[(C_{iii}C_{jjj}C_{ppp})^{\frac{1}{3}}k_i m_i\, k_j m_j]]] \quad (19)$$

As mentioned earlier, in this work, one permeating cryoprotectant (p) and one non-permeating solute, (N), are available in the extracellular solution for the permeating CPA runs. The intracellular solution contains the permeating cryoprotectant and all the native compounds of the cells defined as grouped solute (g). Thus, based on Equation 19 we will have the intra- and extracellular activities:[33]

$$a_p^{in}(t) = \exp\left[ln\left(M_w m_p^{in}(t)\right) + \left(B_{pp} + B_{gg}\right) m_g^{in}(t) + \frac{3}{2}\left(C_{ggg}^2 C_{ppp}\right)^{\frac{1}{3}}\left(\, m_g^{in}(t)\right)^2\right] \quad (20)$$

$$a_p^{ex} = \exp\left[ln\left(M_w m_p^{ex}\right) + \left(B_{pp} + B_{NN}\right) k_N m_N^{ex} + \frac{3}{2}\left(C_{NNN}^2 C_{ppp}\right)^{\frac{1}{3}}\left(\, k_N m_N^{ex}\right)^2\right] \quad (21)$$

In addition, based on equation 5, we can write the intra- and extracellular osmolalities as follows:[33]

$$\pi^{in}(t) = m_p^{in}(t) + m_g^{in}(t) + B_{pp}(m_p^{in}(t))^2 + B_{gg}(m_g^{in}(t))^2 + (B_{pp}+B_{gg})\, m_p^{in}(t)m_g^{in}(t) + C_{ppp}(m_p^{in}(t))^3 + 3(C_{ppp}^2 C_{ggg})^{1/3}(m_p^{in}(t))^2\, m_g^{in}(t) + 3\,(C_{ppp}C_{ggg}^2)^{1/3} m_p^{in}(t)(m_g^{in}(t))^2 + C_{ggg}(m_g^{in}(t))^3 \quad (22)$$

$$\pi^{ex} = m_p^{ex} + k_N m_N^{ex} + B_{pp}(m_p^{ex})^2 + B_{\mathrm{NN}}(k_N m_N^{ex})^2 + (B_{pp}+B_{\mathrm{NN}})\, m_p^{ex} k_N m_N^{ex} + C_{ppp}(m_p^{ex})^3 + 3(C_{ppp}^2 C_{\mathrm{NNN}})^{1/3}(m_p^{in})^2 \mathrm{k_N} m_N^{ex} + 3(C_{ppp}C_{NNN}^2)^{1/3} m_p^{ex}(k_N m_N^{ex})^2 + C_{\mathrm{NNN}}(k_N m_N^{ex})^3 \quad (23)$$

where $m_p^{in}(t)$ and $m_g^{in}(t)$ are the intracellular molalities of the cryoprotectant and the grouped solute, respectively, which are time-dependent and are described as:[33]

$$m_p^{in}(t) = \frac{V_p^{in}(t)\rho_p}{M_p V_w^{in}(t)\rho_w} \quad (24)$$

$$m_g^{in}(t) = \frac{N_g^0}{V_w^{in}(t)\rho_w} \quad (25)$$

where ρ_p is the density of the cryoprotectant, M_p is the molar mass of the cryoprotectant, and N_g^0 is the number of moles of the grouped solutes inside the cell at isotonic conditions. The grouped solute is the non-permeating content of the cell, thus N_g^0 remains constant and is expressed as:[33]

$$N_g^0 = m_g^0 V_{cell}^0 (1 - b^*)\rho_w \quad (26)$$

where m_g^0 is the intracellular molality of the grouped solute at isotonic conditions. m_g^0 can be calculated by writing the Equation 5 for isotonic conditions and then solving it for m_g^0:[33]

$$m_g^0 + B_{gg}\,(m_g^0)^2 + C_{ggg}\,(m_g^0)^3 = \pi^0 \quad (27)$$

The water and cryoprotectant densities are again assumed to be temperature dependent according to Equations 11 and 12. The equations used for the kinetic permeating and non-permeating CPA data fittings are summarized in Table (3) and Table (4), respectively.

Table 3. Equations for modeling the kinetic permeating CPA data

Kinetic **permeating CPA equations** [33,58,60]	
$\frac{dV_w^{in}}{dt} = L_p^* A_{cell}(t) RT \rho_w [\pi^{in}(t) - \pi^{ex}]$	(13)
$\frac{dV_p^{in}}{dt} = P_s^* A_{cell}(t) [a_p^{ex} - a_p^{in}(t)]$	(14)
$L_p^* = L_p^{*RT} \exp[\frac{E_{aLp}}{R} \left(\frac{1}{T_{RT}} - \frac{1}{T}\right)]$	(15)
$P_s^* = P_s^{*RT} \exp[\frac{E_{aPs}}{R} \left(\frac{1}{T_{RT}} - \frac{1}{T}\right)]$	(16)
$A_{cell}(t) = 4\pi \, [\frac{3}{4\pi} V_{cell}(t)]^{2/3}$	(17)
$V_{cell}(t) = V_w^{in}(t) + V_p^{in}(t) + b^* V_{cell}^0$	(18)
$a_p^{in}(t) = \exp\left[ln\left(M_w m_p^{in}(t)\right) + \left(B_{pp} + B_{gg}\right) m_g^{in}(t) + \frac{3}{2}\left(C_{ggg}^2 C_{ppp}\right)^{\frac{1}{3}} \left(m_g^{in}(t)\right)^2\right]$	(20)
$a_p^{ex} = \exp\left[ln\left(M_w m_p^{ex}\right) + \left(B_{pp} + B_{NN}\right) k_N m_N^{ex} + \frac{3}{2}\left(C_{NNN}^2 C_{ppp}\right)^{\frac{1}{3}} (k_N m_N^{ex})^2\right]$	(21)
$\pi^{in}(t) = m_p^{in}(t) + m_g^{in}(t) + B_{pp}(m_p^{in}(t))^2 + B_{gg}(m_g^{in}(t))^2 + (B_{pp}+B_{gg}) m_p^{in}(t) m_g^{in}(t) + C_{ppp}(m_p^{in}(t))^3$ $+ 3(C_{ppp}^2 C_{ggg})^{1/3}(m_p^{in}(t))^2 m_g^{in}(t) + 3 (C_{ppp} C_{ggg}^2)^{1/3} m_p^{in}(t)(m_g^{in}(t))^2 + C_{ggg}(m_g^{in}(t))^3$	(22)

$\pi^{ex} = m_p^{ex} + k_N m_N^{ex} + B_{pp}(m_p^{ex})^2 + B_{\mathrm{NN}}(k_N m_N^{ex})^2 + (Bpp+B_{\mathrm{NN}})\, m_p^{ex} k_N m_N^{ex} + C_{ppp}(m_p^{ex})^3 +$ $3(C_{ppp}^2 C_{\mathrm{NNN}})^{1/3}(m_p^{in})^2 \mathrm{k_N} m_N^{ex} + 3(C_{ppp} C_{NNN}^2)^{1/3} m_p^{ex}(k_N m_N^{ex})^2 + C_{\mathrm{NNN}}(k_N m_N^{ex})^3$ (23)
$m_p^{in}(t) = \frac{V_p^{in}(t)\rho_p}{M_p V_w^{in}(t)\rho_w}$ (24)
$m_g^{in}(t) = \frac{N_g^0}{V_w^{in}(t)\rho_w}$ (25)
$N_g^0 = m_g^0 V_{cell}^0 (1-b)\rho_w$ (26)
$m_g^0 + B_{gg}\,(m_g^0)^2 + C_{ggg}\,(m_g^0)^3 = \pi^0$ (27)
$\rho_w = 999.974950 \times 10^{-18}\left[1 - \frac{(T-3.983035)^2(T+301.797)}{522528.9(T+6934881)}\right]$ (11)[58]
$\rho_p = -9.87181 \times 10^{-19} T + 1.11979 \times 10^{-15}$ (12)[60]

Table 4. Equations for modeling the equilibrium non-permeating CPA data

Kinetic **non-permeating CPA equations**[33,58]
$\frac{dV_w^{in}}{dt} = L_p^* A_{cell}(t) RT \rho_w [\pi^{in}(t) - \pi^{ex}]$ (13)
$L_p^* = L_p^{*RT} \exp[\frac{E_{aLp}}{R}\left(\frac{1}{T_{RT}} - \frac{1}{T}\right)]$ (15)
$A_{cell}(t) = 4\pi\,[\frac{3}{4\pi} V_{cell}(t)]^{2/3}$ (17)
$V_{cell}(t) = V_w^{in}(t) + b^*\, V_{cell}^0$ (18)
$\pi^{in}(t) = m_g^{in}(t) + B_{gg}(m_g^{in}(t))^2\, C_{ggg}(m_g^{in}(t))^3$ (22)
π^{ex} is measured experimentally with an osmometer (23)
$m_g^{in}(t) = \frac{N_g^0}{V_w^{in}(t)\rho_w}$ (25)
$N_g^0 = m_g^0 V_{cell}^0 (1-b^*)\rho_w$ (26)

$m_g^0 + B_{gg}\,(m_g^0)^2 + C_{ggg}\,(m_g^0)^3 = \pi^0$	(27)
$\rho_w = 999.974950 \times 10^{-18}\left[1 - \frac{(T-3.983035)^2(T+301.797)}{522528.9(T+6934881)}\right]$	(11)[58]

2.2.6. Kinetic fitting method

The b^*, B_{gg}, and C_{ggg} values obtained from the equilibrium part are used to fit the kinetic non-permeating CPA data to the equations summarized in Table (4) to obtain L_p^*. Then, the obtained L_p^* along with the three previously calculated parameters are used to fit the permeating CPA data to the equations summarized in Table (3) to obtain P_s^*.

One additional adjustment for the kinetic cell volume data over time was also required before solving the kinetic part for L_p^* and P_s^*. Even though small, there is always a gap between the time of addition of the cell suspension to the solutions (t_0) in a 20 ml vial, and the time that the first few cells pass through the Coulter® counter's aperture (t_1). Thus, t_0 is obtained for each kinetic run and a new time set is generated by replacing t_1 with t_0. Then, the cell volume data over time is adjusted and renewed with the new set of times. After adjusting the data for the time gap, all three repeats of each non-permeating CPA and permeating CPA runs are combined to have one combined set of data for each of them. The combined cell volume data is used to do the kinetic fittings to obtain L_p^* and P_s^*. Then, the time gap fitting is repeated using the obtained L_p^* and P_s^* values to recalculate t_0 for each experimental run. If the new t_0 for each run is not equal to the initially calculated one, each kinetic run will be readjusted with its new time gap, and the kinetic fitting will be redone using the new combined kinetic data to obtain the final values for L_p^* and P_s^*. In addition to the combined data, the kinetic fitting was done for each repeat separately to calculate the error bars for the permeability parameters, L_p^* and P_s^*. The time gap adjustment enables

including the time during which osmotic changes happened to the cells from the moment they touched the hypertonic solution, even before the Coulter® counter recorded any reading, making the experimental data more real and the fittings more accurate.

A flowchart of the kinetic fitting method is given in Figure 8. The parameters involved in this work are also summarized in Table (5), based on whether they change during an experimental run or remain constant. The experimental kinetic data also contain the equilibrium data to increase the accuracy of the kinetic fittings. Ultimately, having L_p^* and P_s^* at room temperature and 0 ºC, their temperature dependence is obtained by taking the room temperature parameters as the reference points and calculating the activation energies, $E_{aL_p^*}$ and $E_{aP_s^*}$ using Equations 15, 16.

The time gap was calculated for each kinetic run in MATLAB using two separate programs for non-permeating CPA and permeating CPA runs. These programs find the time gap by minimizing the sum of squared errors of the non-permeating CPA and permeating CPA codes using a for loop that changes t_0 values. The sum of squared errors was calculated as follows:

$$\text{Error} = \sum\left(\frac{V_{Cell}}{V_0} - \frac{V_{data}}{V_0}\right)^2 \tag{28}$$

where $\frac{V_{Cell}}{V_0}$ is the relative theoretical cell volume and $\frac{V_{data}}{V_0}$ is the relative experimental cell volume. The time gap programs fit data using the b^*, B_{gg}, and C_{ggg}, obtained from the equilibrium fittings, and defining the permeability parameters, L_p^* and P_s^*, as the fitting parameters to be obtained during the run. The time data points column was created again in each run of the loop by adjusting the t_0 values and using the same intervals of the experimental values until the error defined as Equation 28 reaches the set threshold. The error threshold was set manually according to the calculated error by MATLAB; if the calculated error was smaller than the set threshold, a smaller

threshold value was assigned to minimize the error. After finding the time gap, the actual time when the cells touched the solution (t_0) replaced the time they passed the aperture the (t_1), and the time data points column was regenerated.

Two separate programs were written to fit the kinetic experimental data to the model to obtain the permeability parameters, L_p^* and P_s^*, without any iteration between them. The first program was written to solve for L_p^* by fitting the non-permeating CPA experimental data to Equation 13, and the second one was written to solve for P_s^* by fitting the permeating CPA experimental data to Equations 13 and 14, having the L_p^* value from the first code. Both programs conducted the curve-fitting using the MATLAB built-in function "lsqcurvefit" , which is a nonlinear least-square solver that changes the values of the fitting parameters, here L_p^* and P_s^*, to minimize the sum of the squares of residuals of the fit to the experimental data. Since Equations 13 and 14 are ordinary differential equations (ODE), the built-in function "ode45" which solves non-stiff differential equations was used to integrate Equation 13 in the non-permeating CPA program and the system of Equations 13 and 14 in the permeating CPA program. The output of "ode45" is the input of the fitting function "lsqcurvefit" alongside with the experimental cell volume data versus time, and the outputs of the fitting function "lsqcurvefit" are the fitting parameters, L_p^* and P_s^* in the non-permeating CPA and permeating CPA programs, respectively. In these codes, the values of the isotonic and hypertonic extracellular osmolalities, the molality of the Me_2SO and NaCl, b^*, B_{gg} and C_{ggg} were given as known parameters. In each of the kinetic programs, the error between the experimental data and the theoretical model was calculated using the inner option of the 'lsqcurvefit" function, "resnorm", for the comparison purposes between the two aforementioned possible values for C_{ggg} (zero or not zero) to find the best fits.

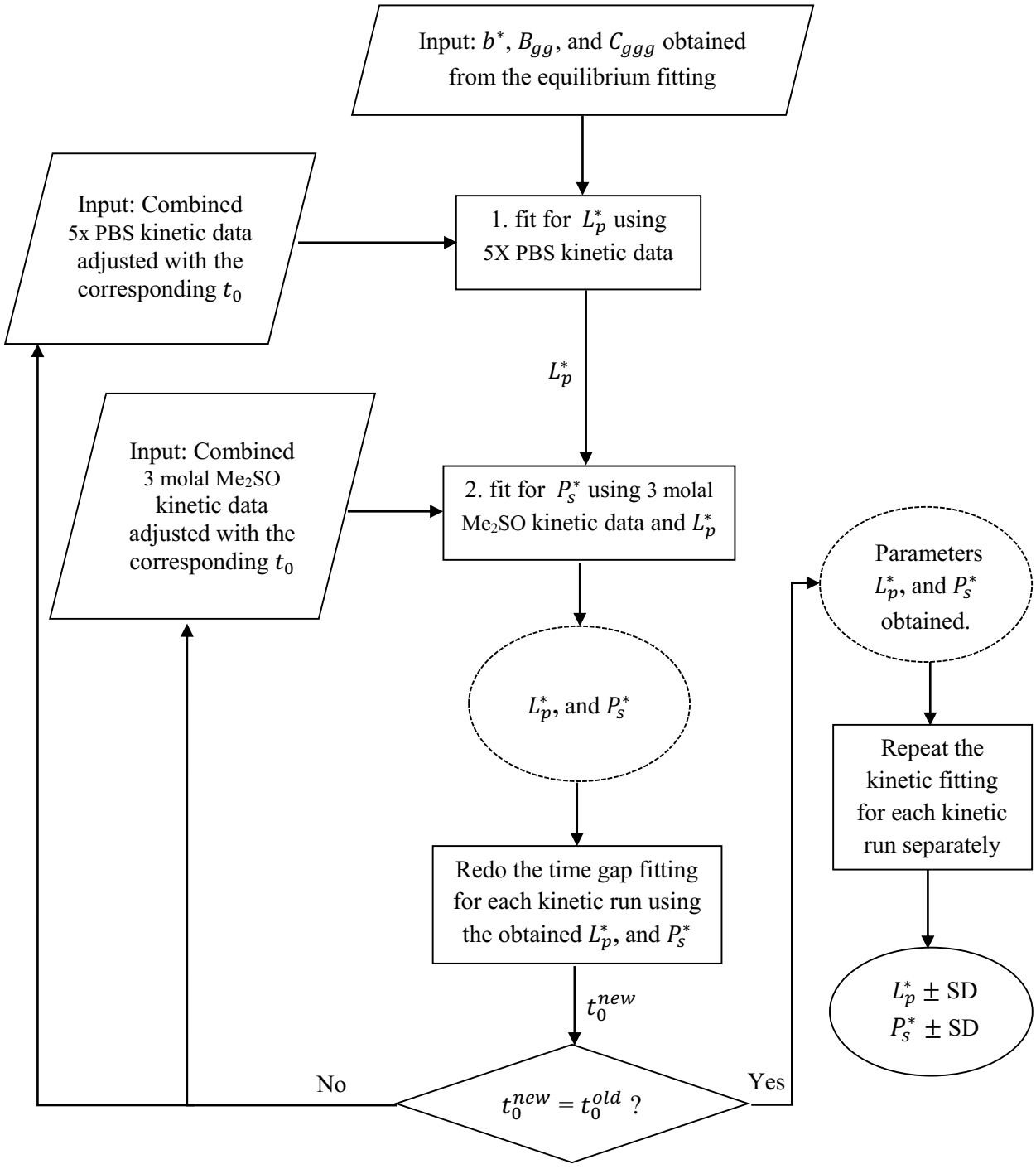

Figure 8. Flowchart of the kinetic fitting method for obtaining the permeability parameters L_p^*, and P_s^* using the obtained parameters from the equilibrium fitting.

Table 5. Parameters (Adapted from reference [34])

Name	description	Value/Unit	Status during a run
V_{cell}	Volume of the cell	μm^3	Variable
V_{cell}^0	Isotonic volume of the cell	μm^3	Constant
V_w^{in}	Intracellular volume of water	μm^3	Variable
V_p^{in}	Intracellular volume of cryoprotectant	μm^3	Variable
m_g^{in}	Intracellular molality of the grouped solute	mole/(kg water)	Variable
m_g^0	Intracellular molality of the grouped solute at isotonic condition	mole/(kg water)	Constant
N_g^0	Intracellular number of moles of the grouped solute at isotonic conditions	mole	Constant
m_p^{in}	Intracellular molality of the cryoprotectant	mole/(kg water)	Variable
m_p^{ex}	Extracellular molality of the cryoprotectant	mole/(kg water)	Constant
m_N^{ex}	Extracellular molality of NaCl	mole/(kg water)	Constant
k_N	Dissociation constant of NaCl[62]	1.678	Constant
b^*	Osmotically inactive fraction of the cell, fitting parameter	–	Constant
ρ_w	Density of water	$kg/\mu m^3$	Constant
ρ_p	Density of the cryoprotectant	$kg/\mu m^3$	Constant
A_{cell}	Surface area of the cell	μm^2	Variable
L_p^*	Hydraulic conductivity	µm/(atm min)	Constant
P_s^*	Cryoprotectant permeability	µm/min	Constant
L_p^{*RT}	Reference value of L_p^* at room temperature	µm/(atm min)	Constant
P_s^{*RT}	Reference value of P_s^* at room temperature	µm/min	Constant
E_{aPs}	Activation energy of P_s^* temperature dependence	kcal/mol	Constant
E_{aLp}	Activation energy of L_p^* temperature dependence	kcal/mol	Constant
π^{in}	Intracellular osmolality	osm/(kg water)	Variable
π^{ex}	Extracellular osmolality	osm/(kg water)	Constant
π^0	Isotonic osmolality, measured	osm/(kg water)	Constant

B_{gg}	Second osmotic virial coefficient of the grouped solute, fitting parameter	(kg water)/mol	Constant
C_{ggg}	Third osmotic virial coefficient of the grouped solute, fitting parameter	((kg water)/mol)^2	Constant
B_{pp}	Second osmotic virial coefficient of the cryoprotectant[62]	0.108 (kg water)/mol	Constant
C_{ppp}	Third osmotic virial coefficient of the cryoprotectant[62]	0 ((kg water)/mol)^2	Constant
B_{NN}	Second osmotic virial coefficient of NaCl[62]	0.044 (kg water)/mol	Constant
C_{NNN}	Third osmotic virial coefficient of NaCl[62]	0 ((kg water)/mol)^2	Constant
M_p	Molar mass of the cryoprotectant[63]	0.078133 kg/mol	Constant
M_w	Molar mass of water[59]	0.01802 kg/mol	Constant
T_{RT}	Room temperature (measured)	K	Constant
T	Temperature (measured)	K	Constant
R	Universal gas constant[64]	82.06×10^{12} $\mu m^3\ atm/(K\ mol)$	Constant
t	Time	min	Variable

Chapter 3. Results

The methods used in this work to minimize the temperature variations during the experimental runs at room temperature and 0 ºC were successful. The temperature range for room temperature experiments was 23.1 ºC – 23.7 ºC, and for 0 ºC experiments was 0.0 ºC – 0.6 ºC for all the cell types, which proves the effectiveness of the methods used in this work compared to the previous work by Gabler Pizarro[34] in which the temperature of the 0 ºC experiments varied from 0.7 ºC to 7.9 ºC during one experimental run according to her lab notebook, and an average value of 4 ºC $\pm$ 0.5 ºC was used for the fittings.

The isotonic cell diameter measured with at least two repeats during the cell preparation process at room temperature using the Coulter® Z2™ counter is reported in Table (6) for all the cell types. These values were used to determine the size of the calibration beads and the Coulter® ZB1™ counter tube for the volume experiments.

Table 6. The measured isotonic diameter of the cells using the Coulter® Z2™ Counter during the cell preparation process at room temperature, and their corresponding calculated volumes. (The values for H9c2 cells, PCECs, hCMECs, and Jurkat cells are measured by Leah Marquez-Curtis.)

Cell types	**HUVECs**	**H9c2 cells**	**PCECs**	**hCMECs**	**Jurkat cells**
Measured diameters (μm)	15.0 $\pm$ 0.75	16.6 $\pm$ 0.6	15.2 $\pm$ 0.65	15.0 $\pm$ 0.25	11.5 $\pm$ 0.55
Calculated volumes (μm^3)	1767 $\pm$ 278	2395 $\pm$ 269	1839 $\pm$ 246	1767 $\pm$ 90	796 $\pm$ 130

The measured isotonic volumes of the cells on each day of experiment using the Coulter® ZB1™ counter and the McGann Cell Size Analyzer program, which were used to generate the relative cell volume data as defined in section 2.2, are also reported in Table (7) for the five cell types at room temperature and 0 ºC. Isotonic runs were conducted three times each day to calculate the

error bars. For some cell types, the 5x PBS and 3 molal Me_2SO runs were performed in one day of experiments, and for other cell types the 5x PBS and 3 molal Me_2SO runs were conducted on two different days, depending on the length of the experiments and the availability of the cells.

Table 7. The measured isotonic volumes of the cells (in μm^3) using the Coulter® ZB1™ Counter and the Cell Size Analyzer program at room temperature and 0 ºC.

Runs		**HUVECs**	**H9c2 cells**	**PCECs**	**hCMECs**	**Jurkat cells**
5x PBS runs' day	**RT**	2159.7 ± 10.8	2280.2 ± 4.7	1813.6 ± 3.1	1691.5 ± 30.1	836.1 ± 20.4
	0 ºC	2010.2 ± 36.3	2336.1 ± 13.2	1789.6 ± 8.1	1568.2 ± 34.3	746.8 ± 23.3
3 molal Me_2SO runs' day	**RT**	2159.7 ± 10.8	2512.5 ± 17.8	1813.6 ± 3.1	1691.5 ± 30.1	836.1 ± 20.4
	0 ºC	2167.8 ± 10.5	2475.3 ± 7.1	1795.8 ± 9.1	1568.2 ± 34.1	744.3 ± 21.2

The time required by each cell type to reach equilibrium that was found using the method described in section 2.2.3 is reported in Table (8). Jurkat cells' permeability to Me_2SO was drastically influenced by lowering the temperature compared to the other cell types. The time required by PCECs to reach equilibrium in 5x PBS solution was not affected by the low temperature as much as the other cells' were.

Table 8. Required time (in minutes) to reach equilibrium for the five cell types at room temperature (RT) and 0 ºC.

Runs	*temperature*	**HUVECs**	**H9c2 cells**	**PCECs**	**hCMECs**	**Jurkat cells**
5x PBS runs	**RT**	0.5	0.4	0.3	0.4	0.3
	0˚C	2.5	2	0.5	2	1
3 molal Me_2SO runs	**RT**	7.5	6	5.5	7	8
	0˚C	12.5	11.5	9.5	13	21.5

The viabilities of all the cell types measured by trypan blue assessment with different durations of exposure to the hypertonic solutions comparable to the duration of the experimental runs are reported in Table (9) at room temperature and 0 ºC.

Table 9. Viabilities of the cell types measured by trypan blue assessment with different durations of exposure to the hypertonic solutions at room temperature (RT) and 0 ºC.

Temperature	Solution	Exposure duration (min)	**HUVECs**	**H9c2 cells**	**PCECs**	**hCMECs**	**Jurkat cells**
RT	5x PBS	1	100%	100%	100%	100%	99.5%
		2	100%	100%	99.5%	99.8%	98.5%
		3	99.3%	99.7%	_	98.3%	94.8%
	3 molal Me_2SO	5	100%	_	100%	_	_
		6	_	98.8%	100%	100%	99.05%
		7	99.3%	98.9%	99.7%	100%	100%
		9	98.6%	97.8%	_	98.9%	96.5%
0 ºC	5x PBS	1	100%	100%	100%	100%	100%
		2	100%	98.5%	100%	99.5%	99%
		3	100%	95.4%	_	98.9%	93.5%
	3 molal Me_2SO	8	_	_	100%	_	_
		9	100%	99.3%	99.6%	100%	_
		11	100%	100%	98.9%	99.65%	_
		13	99.1%	99.1%	_	99.35%	97.7%
		18	_	_	_	_	95%
		20	_	_	_	_	94.8%
Negative control			0.03%				

The fitting method was applied for the five cell types in MATLAB, and the five cell-type-specific parameters were obtained for each cell type. Figures 9 to 13, show the curve fittings of the combined relative volume data in 5x PBS and 3 molal Me_2SO solutions for the five cell types at room temperature and 0 ºC. We observed that adding the data obtained from the equilibrium runs to the kinetic experimental data to conduct the kinetic cell volume fittings reduces the error between the experimental data and the model for 3 molal Me_2SO solutions, resulting in a better fit, and more accurate values for the permeability parameters. Therefore, all the kinetic fittings in this work are done using the combined kinetic and equilibrium experimental data. For 5x PBS the kinetic data is always continued to the equilibrium data without any gap, since the cells reach the equilibrium much faster in this solution.

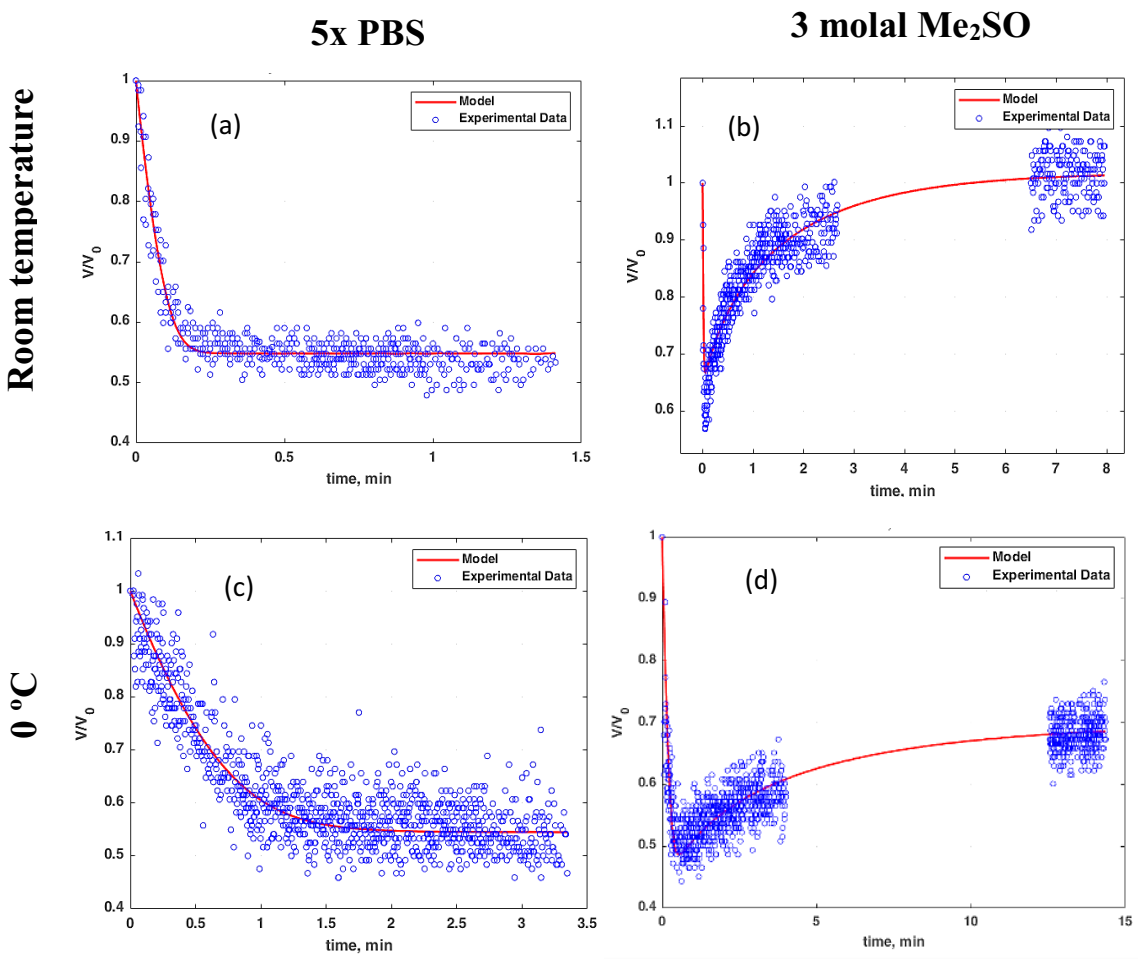

Figure 9. HUVEC experimental data and theoretical model kinetic fits for (a) 5x PBS at room temperature, (b) 3 molal Me_2SO at room temperature, (c) 5x PBS at 0 ºC, and (d) 3 molal Me_2SO at 0 ºC.

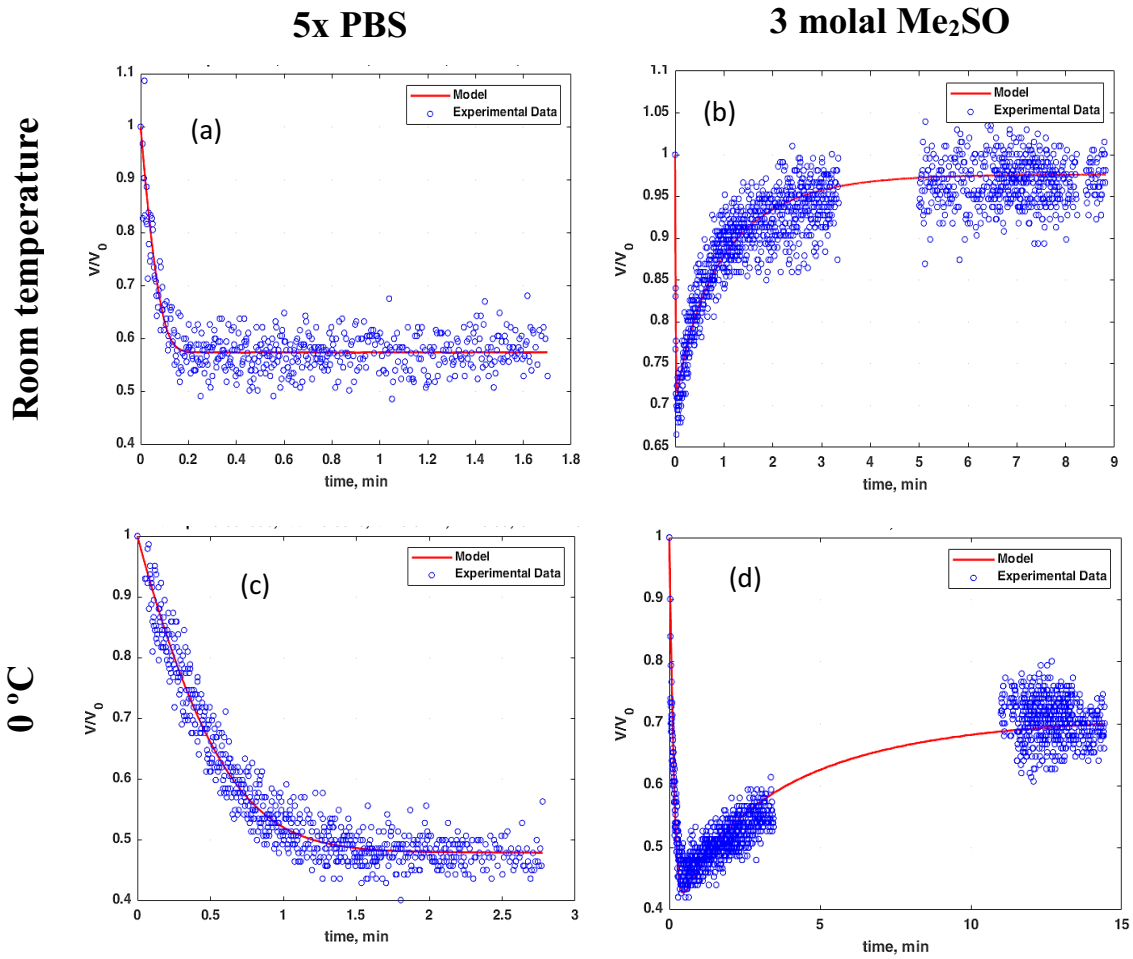

Figure 10. H9c2 cell experimental data and theoretical model kinetic fits for (a) 5x PBS at room temperature, (b) 3 molal Me_2SO at room temperature, (c) 5x PBS at 0 ºC, and (d) 3 molal Me_2SO at 0 ºC.

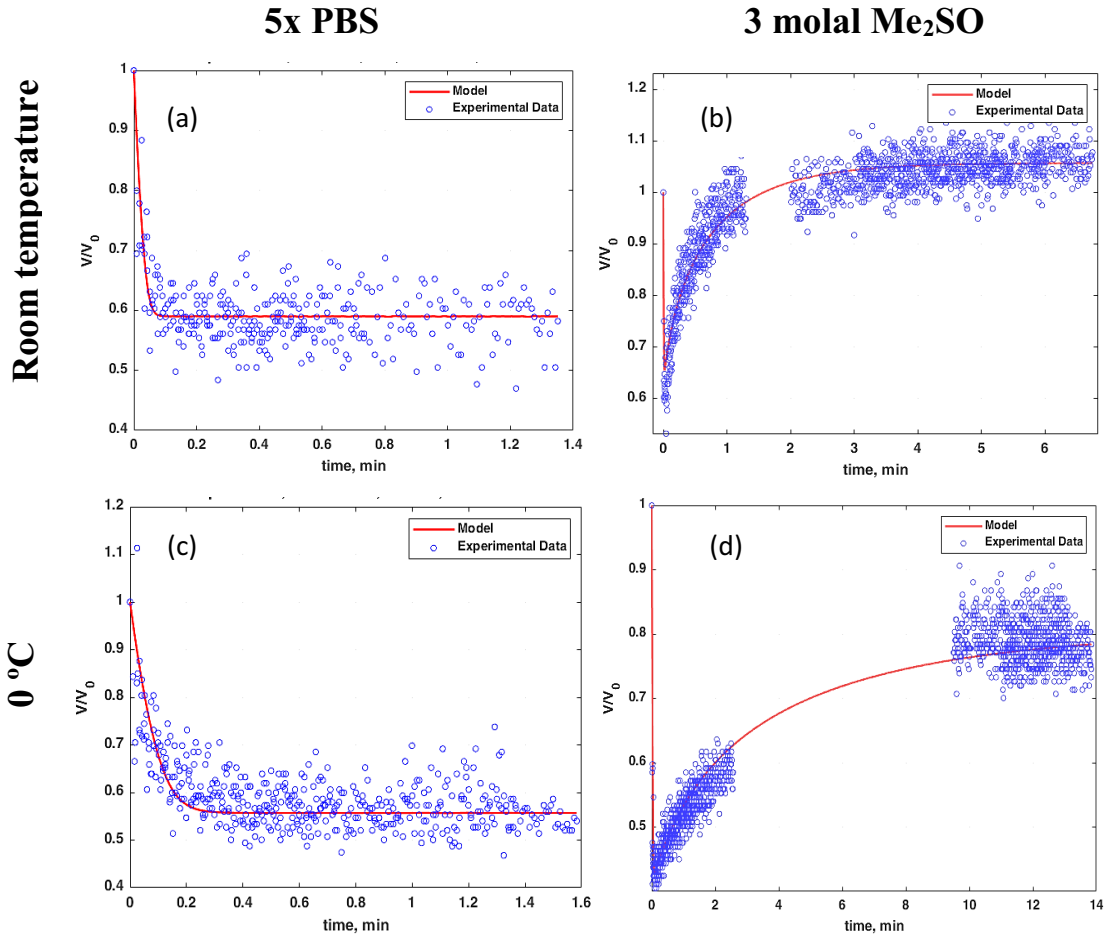

Figure 11. PCEC experimental data and theoretical model kinetic fits for (a) 5x PBS at room temperature, (b) 3 molal Me_2SO at room temperature, (c) 5x PBS at 0 ºC, and (d) 3 molal Me_2SO at 0 ºC.

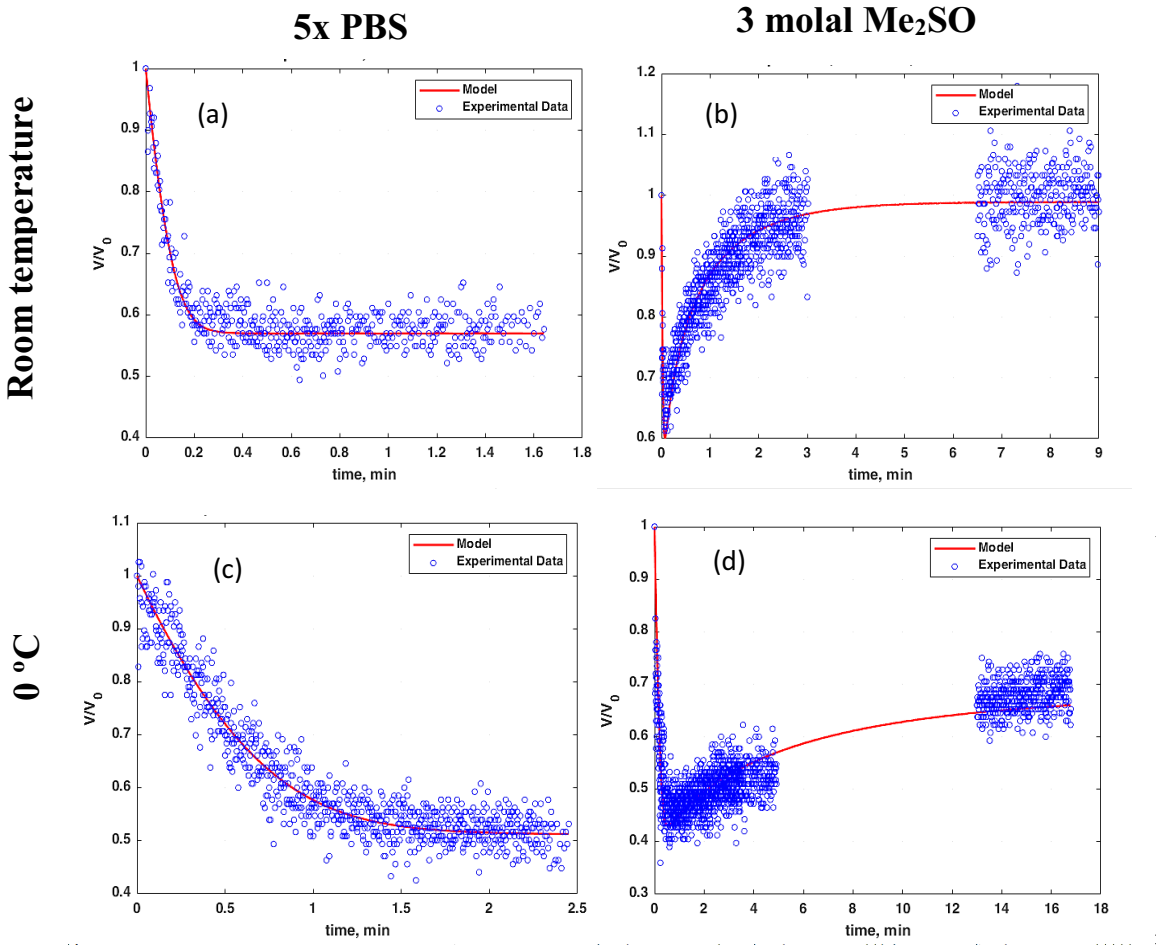

Figure 12. HCMEC experimental data and theoretical model kinetic fits for (a) 5x PBS at room temperature, (b) 3 molal Me_2SO at room temperature, (c) 5x PBS at 0 ºC, and (d) 3 molal Me_2SO at 0 ºC.

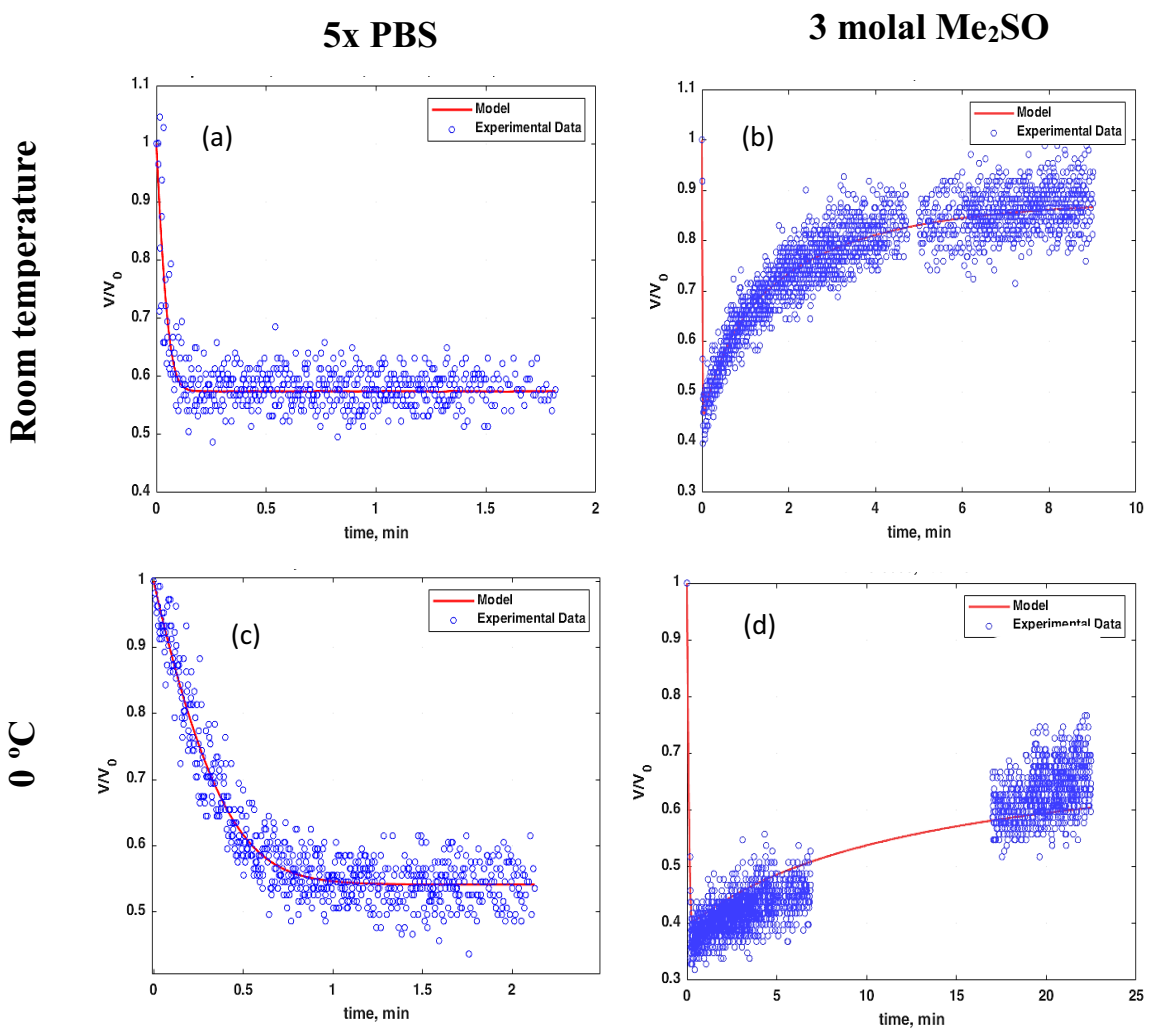

Figure 13. Jurkat cell experimental data and theoretical model kinetic fits for (a) 5x PBS at room temperature, (b) 3 molal Me_2SO at room temperature, (c) 5x PBS at 0 ºC, and (d) 3 molal Me_2SO at 0 ºC.

It was observed for all the cell types that at 0 ºC, the final equilibrium volume of the cells after being in contact with a permeating CPA is considerably smaller than their initial isotonic volume, as indicated in part (d) of Figures 9 to 13. The averages and standard deviations for the five cell-type-specific parameters at room temperature and 0 ºC are reported in Table (10) and Table (11) for the five cell types. Since we used the relative volume data for the fittings (defined in section 2.2), the final result for the L_p^* and P_s^* reported in Table (10) and Table (11) are actually the L_p^* and P_s^* obtained from the fitting methods multiplied by the $V_0^{1/3}$, where V_0 is the measured cell isotonic volume. Statistical t-test analysis was performed in Excel for all the repeats of the room temperature and 0 ºC fitting parameters and the P-values are reported in Table (12). $P < 0.05$ was considered significant. The calculated activation energies related to the Arrhenius equations for modeling the temperature dependence of the cell membrane permeability parameters are also reported in Table (13).

The membrane permeability parameters L_p^*, and P_s^*, for all the cell types decreased significantly by decreasing temperature from room temperature to 0 ºC based on the performed t-test analysis in Excel. At room temperature, HUVECs, H9c2 cells and PCECs data had the best fit when assuming that the third osmotic virial coefficient is equal to zero, but for Jurkat cells and hCMECs that assumption did not lead to the best fit to the experimental data. At 0 ºC on the other hand, for all of the cell types investigated, the third osmotic virial coefficient had a non-zero value in the best fit to the experimental data. For the two cell types that needed the third osmotic virial coefficient both at room temperature and at 0 ºC, Jurkat cells and hCMECs, t-test analysis for the b^*, B_{gg} and C_{ggg} values showed that for both cell types, the $b^*$and B_{gg} values were significantly different at room temperature and 0 ºC, but C_{ggg} value differences were not significant. For all the other cell types, all five cell-type-specific parameters were statistically significantly different at

0 ºC and room temperature. The results of this work clearly indicate that the obtained osmotically inactive fractions of the cells, b^*, are temperature dependent. This observation was consistent for all the cell types studied in this work with different degrees of variation in the value of b^*, suggesting that the cells do not act like perfect osmometers at different temperatures.

Table 10. Means and standard deviations for the cell-type-specific parameters at room temperature

Parameters and units / Cell Type	b^*	B_{gg}	C_{ggg}	L_P^*	P_S^*
	-	kg water / mol	(kg water / mol)^2	μm / atm min	μm / min
HUVECs	0.42 ± 0.03	0.103 ± 0.013	0	0.577 ± 0.089	101.92 ± 18.05
PCECs	0.46 ± 0.01	0.073 ± 0.003	0	1.311 ± 0.407	140.58 ± 42.8
H9c2 Cells	0.449 ± 0.002	0.123 ± 0.007	0	0.584 ± 0.034	130.15 ± 6.21
Jurkat Cells	0.19 ± 0.01	0.65 ± 0.032	24.76 ± 2.26	0.729 ± 0.369	9.45 ± 0.65
hCMECs	0.18 ± 0.02	0.42 ± 0.027	25.7 ± 1.30	0.378 ± 0.013	61.99 ± 2.93

Table 11. Means and standard deviations for the cell-type-specific parameters at 0 ºC

Parameters and units / Cell Type	b^*	B_{gg}	C_{ggg}	L_P^*	P_S^*
	-	kg water / mol	(kg water / mol)^2	μm / atm min	μm / min
HUVECs	0.12 ± 0.05	1.17 ± 0.09	22.84 ± 0.73	0.067 ± 0.002	4.737 ± 0.123
PCECs	0.162 ± 0.028	0.92 ± 0.09	27.44 ± 1.76	0.481 ± 0.159	4.937 ± 1.09
H9c2 Cells	0.017 ± 0.011	0.98 ± 0.07	22.84 ± 1.07	0.102 ± 0.011	7.076 ± 0.448
Jurkat Cells	0.126 ± 0.004	1.1 ± 0.178	23.77 ± 1.18	0.093 ± 0.009	0.527 ± 0.028
hCMECs	0.097 ± 0.024	1.18 ± 0.07	23.61 ± 2.44	0.070 ± 0.009	2.684 ± 0.689

Table 12. P-values of the t-test analysis for the differences between the room temperature and 0 ºC values of the five cell-type-specific parameters (Differences are considered significant when P < 0.05.)

Cell Type	b^*	B_{gg}	C_{ggg}	L_P^*	P_S^*
HUVECs	2.238×10^{-7}	2.324×10^{-10}	3.19×10^{-12}	1.138×10^{-8}	9.371×10^{-6}
PCECs	6.901×10^{-9}	2.388×10^{-9}	2.59×10^{-10}	0.00468	7.591×10^{-6}
H9c2 Cells	1.48×10^{-16}	9.102×10^{-11}	1.853×10^{-13}	1.783×10^{-5}	1.092×10^{-13}
Jurkat Cells	4.301×10^{-5}	0.007674	0.195714	0.01673	1.924×10^{-9}
hCMECs	6.893×10^{-5}	5.286×10^{-6}	0.126294	7.60×10^{-5}	1.593×10^{-13}

Table 13. Means and standard deviations for the cell-type-specific activation energies

Cell Type	$E_{aL_p^*}$ **(kcal/mol)**	$E_{aP_s^*}$ **(kcal/mol)**
HUVECs	14.77 ± 1.68	24.15 ± 6.82
PCECs	7.47 ± 1.89	23.43 ± 2.87
H9c2 Cells	12.36 ± 0.19	21.0 ± 0.37
Jurkat Cells	13.68 ± 3.68	20.41 ± 0.68
hCMECs	12.13 ± 1.11	22.39 ± 1.73

Chapter 4. Using the obtained parameters to model HUVEC volume changes

Now that we have obtained all the cell-type-specific parameters, we can model the cell volume changes during the cryopreservation process using the presented non-ideal thermodynamic model and the commonly used ideal model to investigate the difference. This section illustrates the cell volume model predictions for HUVECs as an example based on the steps of a series of cryopreservation protocols investigated by Sultani et al.[4] In these protocols, the CPA was added to the cells at 0 ºC with at least a 15-minute loading time, and ice nucleation was induced at a subzero temperature between −3 ºC to −5 ºC using precooled forceps in liquid nitrogen followed by a 3-minute holding time to remove the latent heat of fusion. Then, the cell suspensions were slowly (−0.2 °C/min or −1 °C/min) cooled to an intermediate subzero temperature from −25 °C to −40 °C followed by plunging into liquid nitrogen or thawing directly by rapid warming in a 37 °C water bath. The best protocol identified by Sultani et al. was to cool HUVECs at −1 °C/min in the presence of 10% (v/v) Me_2SO or 5% (v/v) Me_2SO plus 6% (v/v) hydroxyethyl starch (HES, a non-permeating CPA) to −35 °C, and then plunge into liquid nitrogen and store.

For the simulations in this work, we assume that the cells are initially at isotonic condition at 0 ºC when 10% (v/v) Me_2SO solution mixed in isotonic NaCl is added to the cell suspension and left to equilibrate for 15 minutes. After CPA loading, the suspension is instantly cooled to −5 ºC, assuming no cell volume changes happen in between. At −5 ºC, ice nucleation is induced. The suspension is held at −5 ºC for 3 minutes after the nucleation and then cooled at −1 ºC/min to −40 ºC. The role of latent heat of fusion is ignored in this simulation. Then, cell suspensions are thawed directly from −40 ºC to 0 ºC by rapid warming. Based on our personal communication with Dr. Leah Marquez-Curtis, who frequently conducts the HUVEC cryopreservation process in our lab, the warming rate related to directly thawing a glass cryovial of HUVECs in a 37 °C water bath

from −40 ºC to 0 ºC is approximately 100 ºC/min (rapid warming). After thawing, the Me_2SO is removed from the cells by diluting the suspensions in an isotonic medium at room temperature. We assume no significant water or CPA movements happen between the thawing to 0 ºC and warming to RT as dilution begins.

The modeling is done in MATLAB, having the five cell-type-specific parameters and the activation energies as known values. For the osmotic parameters, b^*, B_{gg} and C_{ggg}, the values measured at 0 ºC reported in Table (11) are used, except for the dilution step in which the room temperature values reported in Table (10) are used. Permeability parameters, L_P^* and P_S^*, are expressed by their corresponding Arrhenius equations as below:

$$L_P^* = 0.577\exp\left[\frac{14.77}{R}\left(\frac{1}{296.15} - \frac{1}{T}\right)\right] \tag{29}$$

$$P_S^* = 101.91\exp\left[\frac{24.15}{R}\left(\frac{1}{296.15} - \frac{1}{T}\right)\right] \tag{30}$$

For the first step, the CPA loading, the cell volume is modeled using the permeating-CPA kinetic volume equations summarized in Table (3). In this step, the cells initially shrink as water leaves the cells and then swell back up as the permeating CPA, Me_2SO, diffuses into the cells and some water comes back into the cells. The cells finally reach an equilibrium volume within 15 minutes that is smaller than their initial isotonic volume at 0 ºC.

In the second step, ice nucleation is induced at −5 ºC. When the ice is nucleated at −5 ºC, the pure water solidifies, concentrating the extracellular solutes and causing an increase in the extracellular molality of the Me_2SO. Thus, the ice nucleation step acts like a small CPA addition step. The solidification of extracellular water will also increase the salt (NaCl) concentration outside the cells drawing more water out. Therefore, in the presence of ice, we need a new equation to calculate

the extracellular osmolality as a function of freezing temperature. The changing cell volume in the ice nucleation step is modeled using the equations summarized in Table (3), and the extracellular osmolality as a function of the freezing point defined below:[29,62]

$$\pi = \frac{T_m^0 - T_m}{RT_m[M_1/\overline{\Delta S_{f1}^0}]} \tag{31}$$

where T_m is the absolute freezing point of the solution (in Kelvin), T_m^0 is the absolute freezing point of pure water (273.15 K), R is the universal gas constant (8.314 J/mol K), M_1 is the molar mass of water (0.01802 kg/mol), and $\overline{\Delta S_{f1}^0}$ is the standard molar entropy change of fusion of water (22 J/mol K) at the freezing point of pure water. Substituting the values of the constants will result in the following:

$$\pi = \frac{273.15 - T_m}{6.8099\times10^{-3}\, T_m} \tag{32}$$

After the extracellular osmolality at -5 ºC is calculated using Equation 32, the result is used to calculate the new values for the extracellular molalities of the Me_2SO and NaCl using Equation 23, and the ratio of the initial extracellular molalities of Me_2SO and NaCl (which is known and stays constant during the whole process) defined as below:

$$m_{ratio} = m_N^{ex} / m_p^{ex} \tag{33}$$

where m_N^{ex} is the extracellular molality of NaCl, and m_p^{ex} is the extracellular molality of the Me_2SO. The new values of the extracellular molality of the Me_2SO and NaCl are used to calculate the Me_2SO extracellular activity using Equation 21.

In the slow cooling process to -40 ºC, the solidification of extracellular water will increase the extracellular osmolality, drawing more water out. Thus, the changing cell volume is modeled using

the same equations used in the second part and defining the temperature changes over time as below:

$$T = Bt + T_{initial} + 273.15 \quad (34)$$

where B is cooling rate, equal to -1 ºC/min in this case, t is time (min), $T_{initial}$ is the temperature of ice nucleation (in ºC), in this case, -5 ºC, and T is the temperature (in K). At each temperature calculated by Equation 34 in the slow cooling process, the extracellular osmolality is calculated using Equation 32, and the extracellular molality of the Me_2SO and NaCl are calculated using Equations 23 and 33.

In the rapid warming process, as the temperature increases from -40 ºC to 0 ºC, the ice melts and the extracellular osmolality calculated by Equation 32 decreases, which leads to water moving into the cells to remove the chemical potential differential, making the cells swell. The rapid warming process is modeled using the same equations used for the slow cooling process and having B as the warming rate equal to 100 ºC/min, and $T_{initial}$ equal to -40 ºC in Equation 34.

The dilution process is done at room temperature using a solution with no permeating CPA to draw the Me_2SO out of the cells. The larger intracellular osmolality makes the water initially move into the cells, causing an initial swelling. Then, the water moves out of the cells as the Me_2SO leaves the cells, causing shrinkage. The same equations used in the CPA loading process are used to model the dilution process, except with the measured osmotic and permeability values at room temperature. Also, the temperature in the MATLAB code is set to 23.5 ºC, and the extracellular osmolality of the Me_2SO is set to a number very close to zero (0.000001) in order for the code to be able to find an answer.

To calculate the cell-type-specific parameters and the activation energies for the ideal thermodynamic model (reported in Table (14)), the fitting methods were performed based on the most common ideal thermodynamic models, assuming that all the osmotic virial coefficients of the solutes (grouped solute, salt, and CPA) were equal to zero, meaning that the osmolalities were equal to the simple summation of the solute concentrations as indicated below for the non-electrolyte and electrolyte solutes:[62]

$$\pi = \sum_{i=2}^{r} k_i m_i \tag{35}$$

where m_i is the molality of solute i, and k_i is the dissociation constant of the electrolyte solute i, k_i = 1 for non-electrolyte solutes.

The cell-type-specific parameters used for CPA loading, cooling to −40 ºC, and rewarming to 0 ºC are the ones measured at 0 ºC because they are more likely to be accurate under cryobiological conditions. For the dilution step, on the other hand, the room temperature values for the cell-type-specific parameters are used. The cell-type-specific parameters and the activation energies used in both models are reported in Table (14).

Table 14. Cell-type-specific parameters and the activation energies used in the HUVEC models

Non-ideal Parameters		b^*	B_{gg}	C_{ggg}	L_P^*	P_S^*	$E_{aL_p^*}$	$E_{aP_s^*}$
values	**RT**	0.4	0.103	0	0.577	101.92	14.77	24.15
	0˚C	0.12	1.17	22.8	0.067	4.737		
Ideal Parameters		b	B_{gg}	C_{ggg}	L_P	P_S	E_{aLp}	E_{aPs}
values	**RT**	0.4	0	0	0.603	36.473	15.631	19.675
	0˚C	0.4	0	0	0.067	2.297		

The HUVEC volume changes during the preservation process are modeled using the ideal and non-ideal thermodynamic models, which are illustrated in Figure 14 as the changes in the relative volumes of the cell, intracellular water, and intracellular CPA versus time. The relative cell volume is the total relative volumes of the intracellular water and CPA plus the osmotically inactive fraction of the cell.

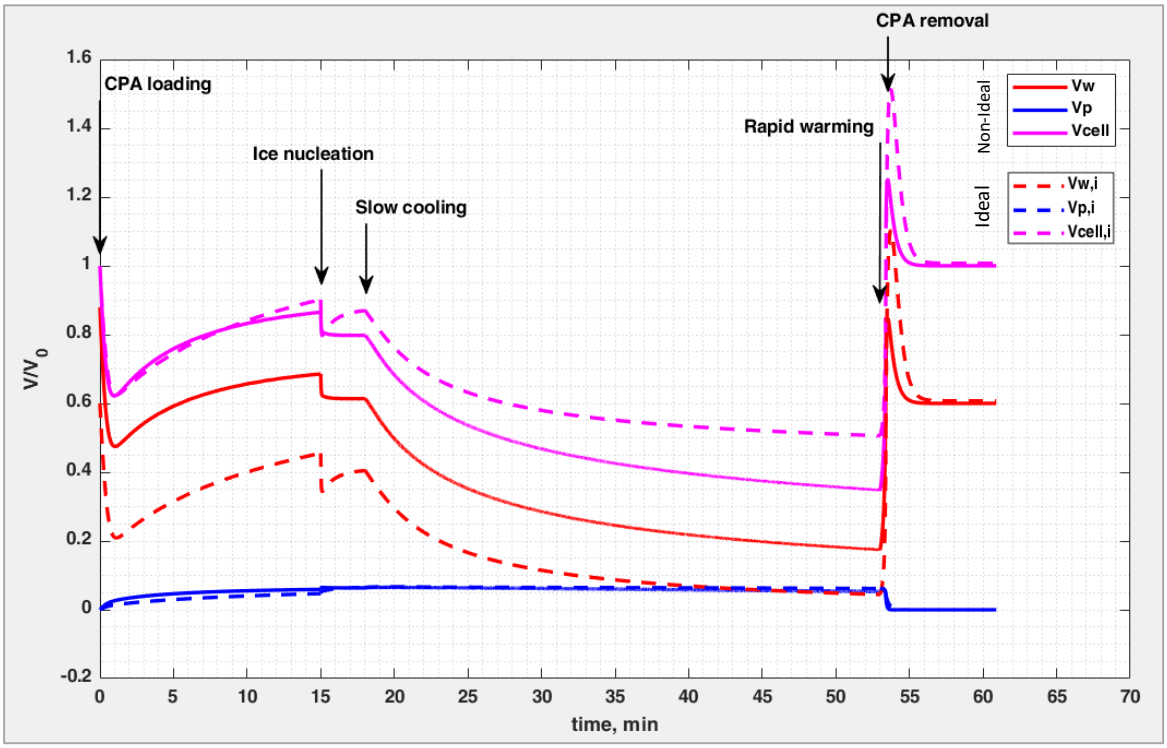

Figure 14. Model predictions for relative volume over time for the HUVEC cryopreservation protocol, representing non-ideal (solid lines) and ideal (dashed lines) models. The magenta lines represent the relative cell volume (V_{cell}), the red lines represent the contribution to the relative volume of intracellular water (V_W), and the blue lines indicate the contribution to the relative volume of intracellular Me_2SO (V_P). Minutes 0 to 15 show the Me_2SO addition step, minutes 15 to 18 show the ice nucleation holding time, minutes 18 to 53 show the slow cooling (-1 ˚C/min) process to -40 ˚C, minutes 53 to 53.4 show the rapid warming (100 ºC/min) process from -40 ˚C to 0 ºC, and minutes 53.4 to 60.9 show the Me_2SO removal step at room temperature.

The calculated cell volume (V_{cell}) and the volume of intracellular water (V_w) and Me_2SO (V_p) for each step of the protocol for both models are also reported in Table (15). Figure 14 indicates that the ideal and non-ideal models have similar overall shapes but predict different values for the

relative volumes in each step of the process. The deviation of the non-ideal model from the ideal model for the intracellular Me_2SO volume is less significant than that for the volume of intracellular water. There is also a small jump in the relative cell volume between the rapid warming and dilution steps for the non-ideal model, which is caused by the temperature dependence of the osmotically inactive fraction of the cells reported in Table (14).

The model predictions play a significant role in cryobiologists' understanding of cell osmotic behavior and designing their optimization methods. Therefore, even the slightest improvement in modeling the changing cell volume using the non-ideal assumptions can make the optimization process much more accurate. For instance, cryobiologists need to minimize the osmotic stress on the cell during the CPA addition, cooling, and CPA removal steps, and for that, they need to have accurate predictions of the cell volume changes in these steps. A bigger change in the cell volume in a certain amount of time leads to larger osmotic stress on the cells. As indicated in Figure 14, the ideal model overestimates the osmotic stress on the cells in the CPA addition and removal, and ice nucleation steps, and significantly underestimates the osmotic stress in the slow cooling process. The other significant difference between the non-ideal and ideal models is their predictions of the osmotically inactive volume of the cells and, consequently, the intracellular water content at different temperatures. The ideal model yields an osmotically inactive fraction equal to 0.4 at 0 ºC, while the non-ideal model yields one equal to 0.1203. That means the ideal model predicts significantly smaller intracellular water content for the cells at sub-zero temperatures. The final volume predictions after the dilution step at room temperature are almost the same for the ideal and non-ideal models.

Table 15. Relative cell, water, and CPA volumes after each step of the cryopreservation process for HUVECs. The matching colors in this table and Table (16), where the effects of protocol deviations are explored, highlight the equal values for the corresponding steps of the protocols.

		using the non-ideal thermodynamic model	**using the ideal thermodynamic model**
Before CPA addition at 0 ºC	V_w^0	0.8797	0.6
	V_p^0	0	0
	V_{Cell}^0	1	1
After CPA loading at 0 ºC for 15 min	V_w^1	0.6857	0.455
	V_p^1	0.0593	0.0471
	V_{Cell}^1	0.8652	0.9021
After ice nucleation at −5 ºC for 3 min	V_w^2	0.6140	0.4046
	V_p^2	0.064	0.065
	V_{Cell}^2	0.7980	0.8698
After slow cooling to −40 ºC	V_w^3	0.1746	0.0443
	V_p^3	0.053	0.0618
	V_{Cell}^3	0.3479	0.5061
After rapid warming to 0 ºC	V_w^4	0.6748	0.5311
	V_p^4	0.034	0.046
	V_{Cell}^4	0.829	0.9771
After CPA removal (at RT)	V_w^5	0.6001	0.6074
	V_p^5	2.67×10^{-7}	1.08×10^{-7}
	V_{Cell}^5	1.000	1.007

In order to have a deeper understanding of how each step of the cryopreservation protocol influences the HUVEC volume changes, the modeling is repeated with four other conditions: i) a protocol with a dilution step done at 0 ºC instead of room temperature (Figure 15). ii) Another protocol with not enough time for CPA loading at the beginning of the process (i.e., 30 seconds)

and cooling the cells almost immediately after adding the CPA (Figure 16). iii) A protocol with a cooling rate equal to -2 ºC/min instead of -1 ºC/min (Figure 17), and iv) a protocol with a cooling rate equal to -10 ºC/min (Figure 18). In each modified protocol, just the mentioned step is changed, and the other steps and conditions are kept the same as in the original protocol. The calculated final cell volume (V_{cell}) and the volume of intracellular water (V_w) and CPA (V_p) for each step related to each protocol are reported in Table (16). The ideal and non-ideal models arrive at the exact same volumes as the original protocol (reported in Table (15)) after slow cooling to -40 ºC for protocols i and ii, after CPA removal (at room temperature) for protocols ii, iii, and iv, and after the rapid warming process to 0 ºC for all the protocols.

Figure 15 shows that in a dilution step done at 0 ºC, the water diffuses into the cells much faster than the CPA moves out of the cells, causing larger cell volume changes and extra osmotic stress compared to a dilution step done at room temperature, which is also demonstrated by the higher water content of the cells after CPA removal for this protocol reported in Table (16) compared to the original protocol reported in Table (15). When the dilution is modeled at 0 ºC, there is no jump in the cell volume between the warming and dilution steps for the non-ideal model since the same value of b^* (0.12) is used for both steps. Figure 15. (a) shows that the ideal model overestimates the osmotic stress on the cells for CPA removal at 0 ºC as well as at room temperature compared to the non-ideal model. As indicated in Figure 15. (b), which compares the original protocol and protocol i, the CPA removal at room temperature happens faster and causes less osmotic stress caused by large kinetic movements on the cells than the CPA removal at 0 ºC for both ideal and non-ideal models.

Figure 16 indicates that when the CPA loading time is short, a sudden CPA loading at the beginning of the ice nucleation step will compensate for it, bringing the cells to the same final

conditions after the cooling, warming, and CPA removal steps. That means successful cryopreservation of the cells is also possible without having a long CPA loading step.

Figure 17 indicates that by having a cooling rate equal to -2 ºC/min, the models predict approximately the same volume values (0.02% error) at -40 ºC and exactly the same values after the rapid warming and dilution steps as the original protocol with a -1 ˚C/min cooling rate, but reaches it in a shorter time, causing larger osmotic stress on the cells.

Based on both ideal and non-ideal models, higher cooling rates will result in larger water contents for the cells at -40 ºC. As indicated in Figure 18 and reported in Table (16), a -10 ˚C/min cooling rate will result in relative intracellular water volumes equal to 0.1748 based on the non-ideal model and equal to 0.0446 based on the ideal model at -40 ºC, which are slightly larger than the values predicted by the original model, which are equal to 0.1746 and 0.0443, respectively. Although the differences between the values predicted by the original ptotocol and by the protocol with a ten times faster cooling rate are not significant, the increasing trend for the intracellular water content shows that high cooling rates can cause low dehydration, leading to a large extent of supercooling and a high probability of intracellular ice formation. Having an accurate prediction of these values using the mathematical model is essential for cryobiologists to be able to maximize cell survival after the cryopreservation process.

The effect of other conditions and variables can be investigated as easily; the role of the intermediate sub-zero temperature, ice nucleation temperature, the permeating CPA concentration, salt concentration, warming rate, and CPA loading or removal steps and temperature can all be studied separately or simultaneously using the presented thermodynamic model.

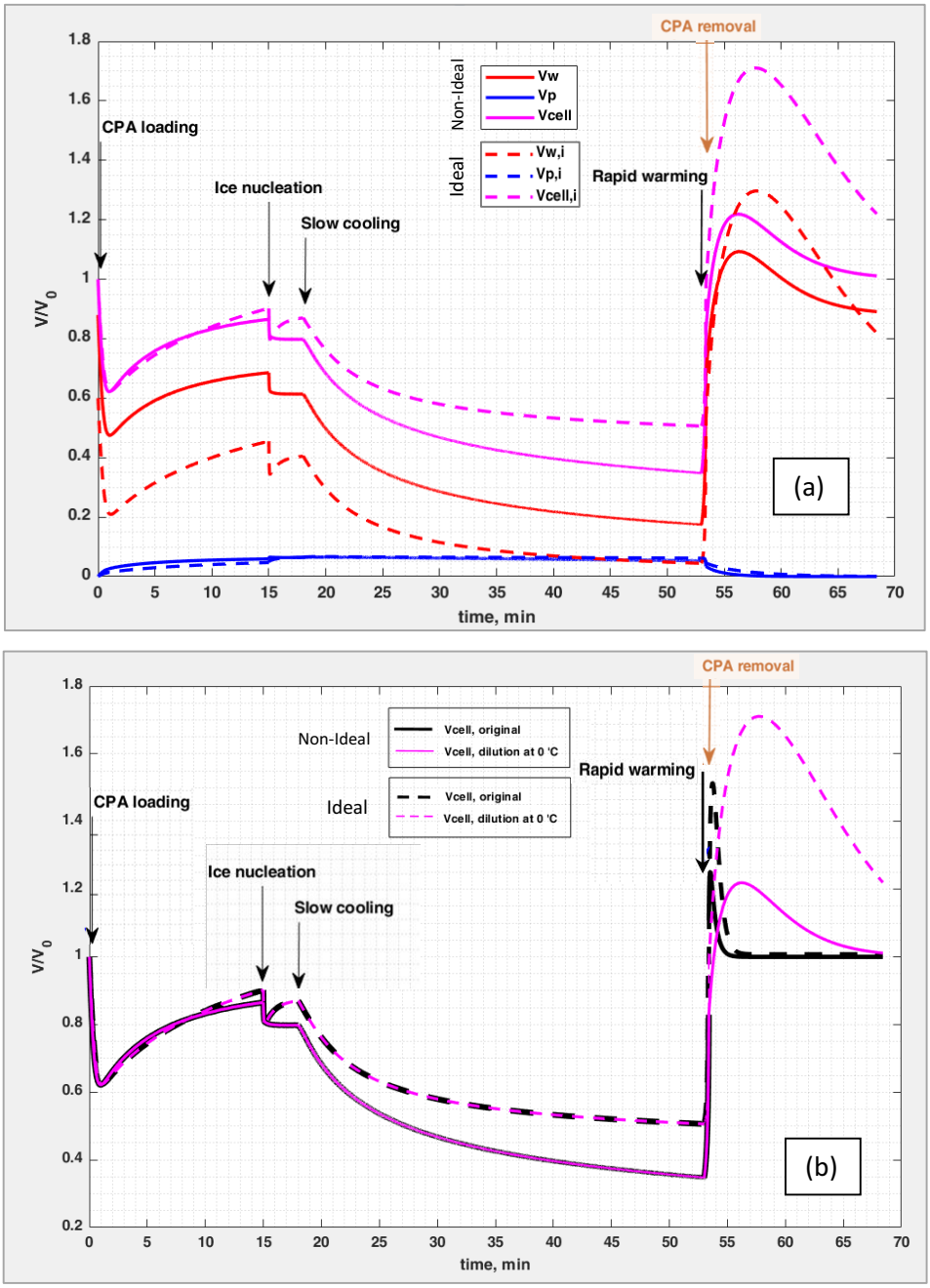

Figure 15. Model predictions for relative volume over time, representing non-ideal (solid lines) and ideal (dashed lines) models, (a) for the HUVEC cryopreservation protocol with dilution at 0 ºC; (b) comparing the protocol with dilution at 0 ºC and the original protocol with dilution at room temperature. The magenta lines represent the relative cell volume (V_{cell}), the red lines represent the contribution to the relative volume of intracellular water (V_W), and the blue lines indicate the contribution to the relative volume of intracellular Me_2SO (V_P) for the protocol with dilution at 0 ºC, and the black lines show V_{cell} for the original protocol with dilution at room temperature. Minutes 0 to 15 show the Me_2SO addition step, minutes 15 to 18 show the ice nucleation holding time, minutes 18 to 53 show the slow cooling (−1 ˚C/min) process to −40 ºC, minutes 53 to 53.4 show the rapid warming (100 ºC/min) process from −40 ˚C to 0 ºC, and minutes 53.4 to 60.9 show the Me_2SO removal step.

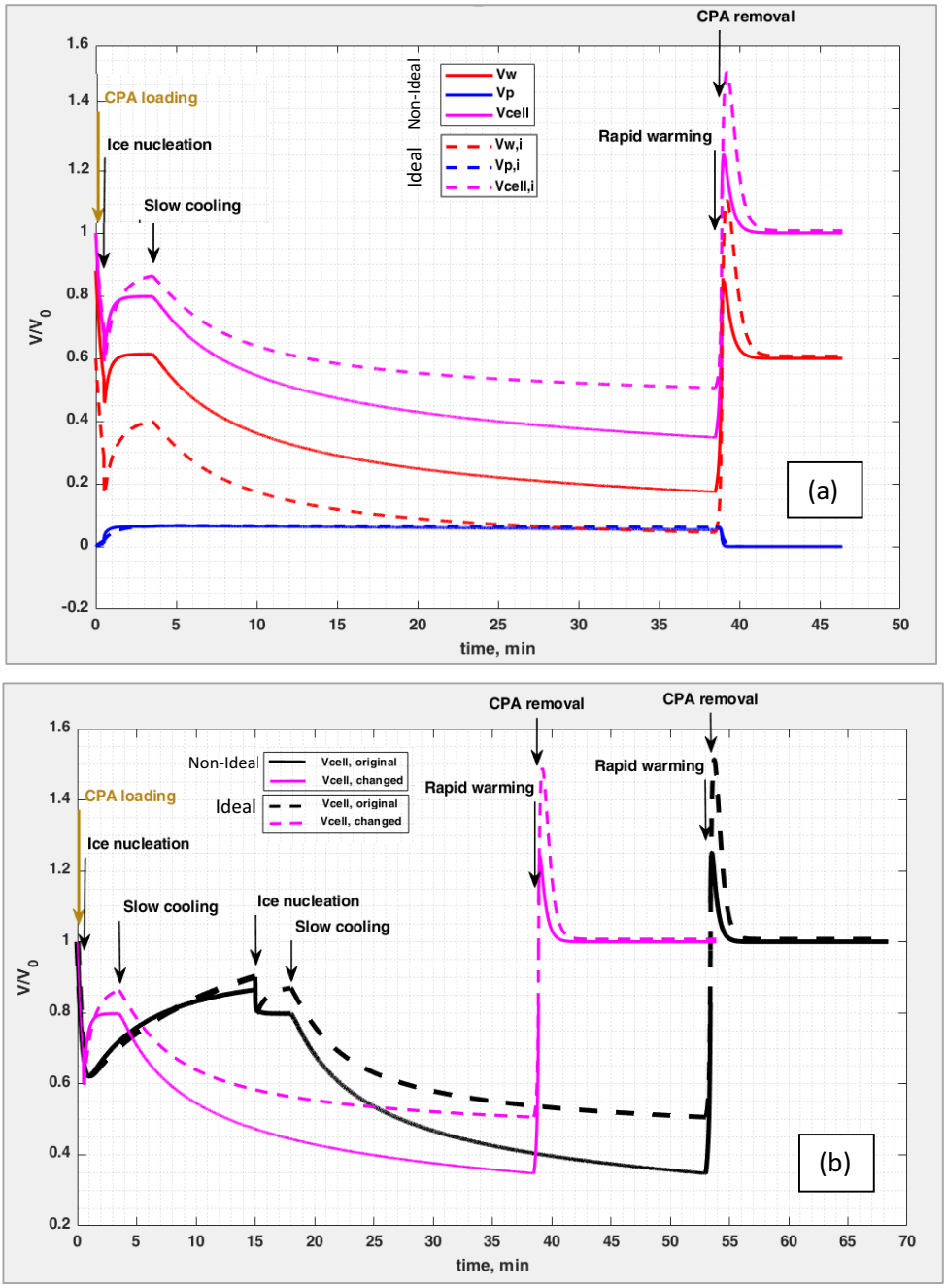

Figure 16. Model predictions for relative volume over time, representing non-ideal (solid lines) and ideal (dashed lines) models, (a) for the HUVEC cryopreservation protocol with not enough incubation time (0.5 min); (b) comparing the protocol with not enough incubation time and the original protocol. The magenta lines represent the relative cell volume (V_{cell}), the red lines represent the contribution to the relative volume of intracellular water (V_W), and the blue lines indicate the contribution to the relative volume of intracellular Me_2SO (V_P) for the protocol with not enough incubation time, and the black lines show V_{cell} for the original protocol with enough incubation time (15 min).

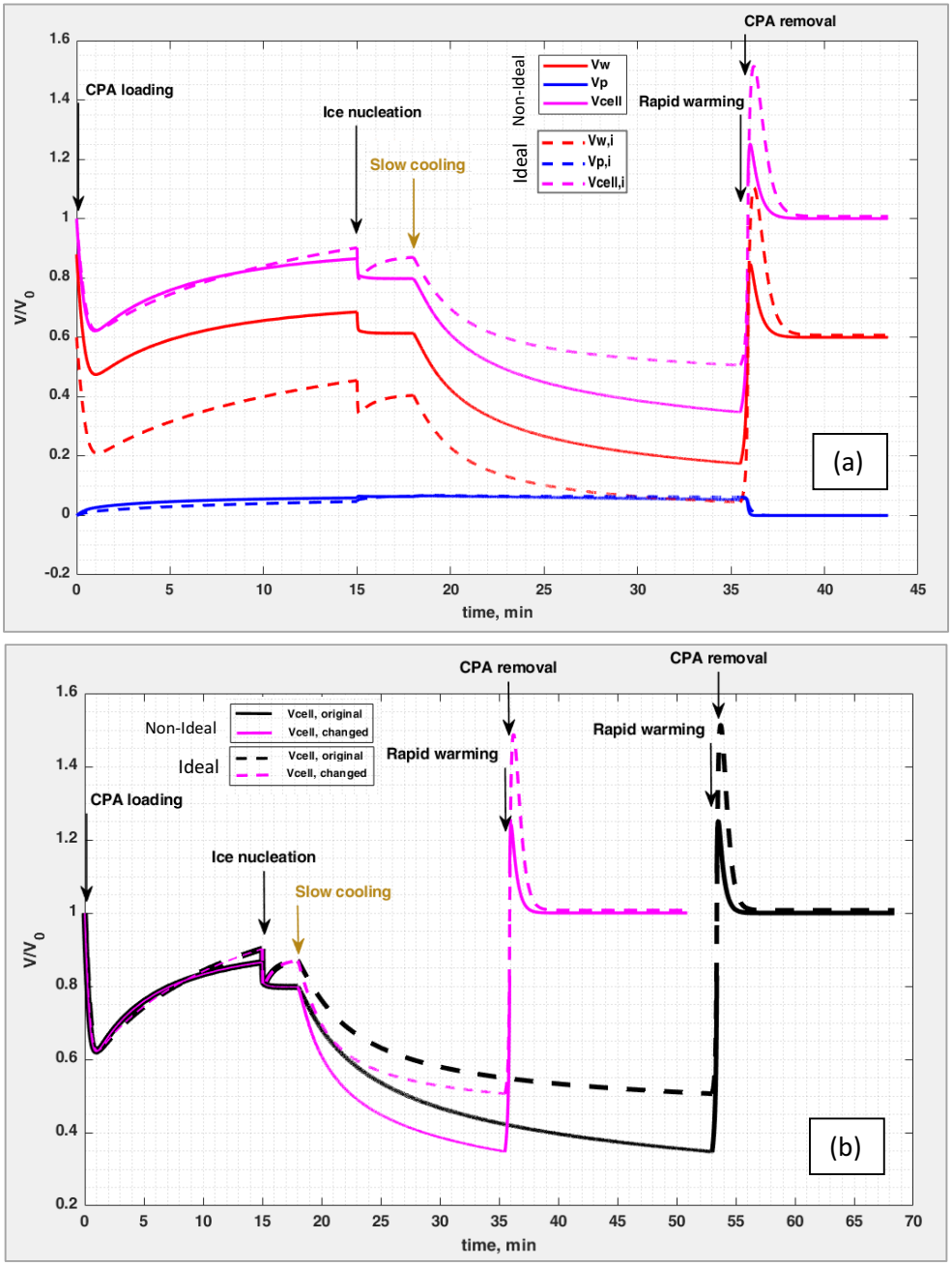

Figure 17. Model predictions for relative volume over time, representing non-ideal (solid lines) and ideal (dashed lines) models, (a) for the HUVEC cryopreservation protocol with −2 ºC/min cooling rate; (b) comparing the protocol with −2 ºC/min cooling rate and the original protocol. The magenta lines represent the relative cell volume (V_{cell}), the red lines represent the contribution to the relative volume of intracellular water (V_W), and the blue lines indicate the contribution to the relative volume of intracellular Me_2SO (V_P) for the protocol with −2 ºC/min cooling rate, and the black lines show V_{cell} for the original protocol with −1 ºC/min cooling rate.

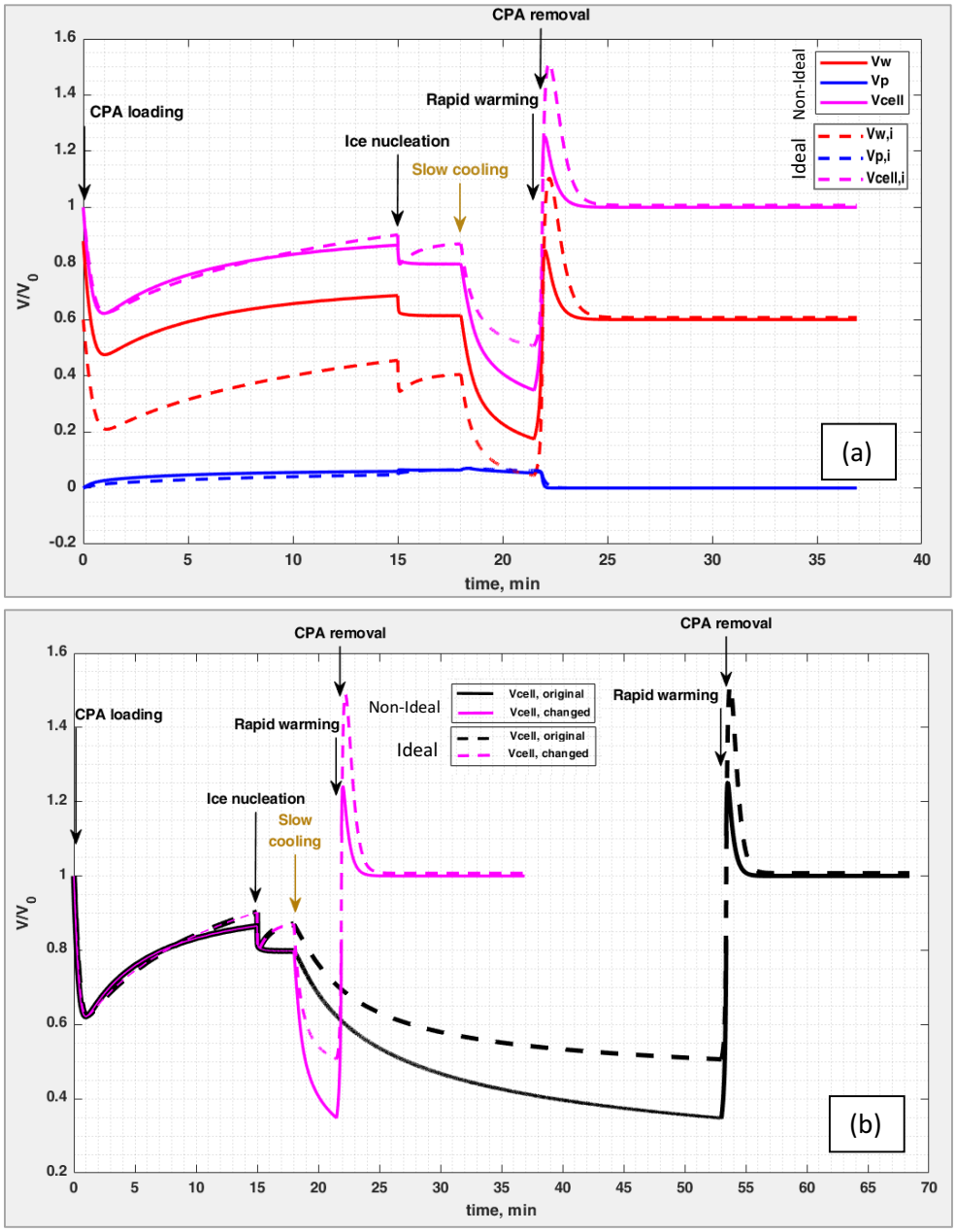

Figure 18. Model predictions for relative volume over time, representing non-ideal (solid lines) and ideal (dashed lines) models, (a) for the HUVEC cryopreservation protocol with −10 ºC/min cooling rate; (b) comparing the protocol with −10 ºC/min cooling rate and the original protocol. The magenta lines represent the relative cell volume (V_{cell}), the red lines represent the contribution to the relative volume of intracellular water (V_W), and the blue lines indicate the contribution to the relative volume of intracellular Me_2SO (V_P) for the protocol with −10 ºC/min cooling rate, and the black lines show V_{cell} for the original protocol with −1 ºC/min cooling rate.

Table 16. Relative cell, water, and CPA volumes after each step of the changed cryopreservation process for HUVECs. The matching colors in this table and Table (15) highlight the equal values for the corresponding steps of the protocols.

		(i) With the dilution step done at 0 ºC		*(ii) With not enough CPA loading time*		*(iii) With −2 ºC/min cooling rate*		*(iv) With −10 ºC/min cooling rate*	
		Non-ideal	***ideal***	***Non-ideal***	***ideal***	***Non-ideal***	***ideal***	***Non-ideal***	***ideal***
Before CPA addition at 0 ºC	V_w^0	0.8797	0.6	0.8797	0.6	0.8797	0.6	0.8797	0.6
	V_p^0	0	0	0	0	0	0	0	0
	V_{Cell}^0	1	1	1	1	1	1	1	1
After CPA loading at 0 ºC for 15 min	V_w^1	0.6857	0.455	0.5386	0.2902	0.6857	0.455	0.6857	0.455
	V_p^1	0.0593	0.0471	0.0185	0.0095	0.0593	0.0471	0.0593	0.0471
	V_{Cell}^1	0.8652	0.9021	0.6774	0.6997	0.8652	0.9021	0.8652	0.9021
After Ice nucleation at −5 ºC for 3 min	V_w^2	0.6140	0.4046	0.6143	0.3993	0.6140	0.4046	0.6140	0.4046
	V_p^2	0.0638	0.0652	0.064	0.0642	0.0638	0.0652	0.0638	0.0652
	V_{Cell}^2	0.7980	0.8698	0.7983	0.8634	0.7980	0.8698	0.7980	0.8698
After slow cooling to −40 ºC	V_w^3	0.1746	0.0443	0.1746	0.0443	0.1746	0.0444	0.1748	0.0446
	V_p^3	0.053	0.0618	0.053	0.0618	0.053	0.0618	0.0531	0.0621
	V_{Cell}^3	0.3479	0.5061	0.3479	0.5061	0.3480	0.5062	0.3482	0.5066
After rapid warming to 0 ºC	V_w^4	0.6748	0.5311	0.6748	0.5311	0.6748	0.5311	0.6748	0.5311
	V_p^4	0.034	0.046	0.034	0.046	0.034	0.046	0.034	0.046
	V_{Cell}^4	0.829	0.9971	0.829	0.9771	0.829	0.9771	0.829	0.9771
After CPA removal (at RT)	V_w^5	0.8909	0.8191	0.600	0.607	0.600	0.607	0.600	0.607
	V_p^5	0.000	0.000	0.000	0.000	0.000	0.000	0.000	0.000
	V_{Cell}^5	1.011	1.219	1.000	1.007	1.000	1.007	1.000	1.007

Chapter 5. General discussion

The importance of this work is that no other previous research has obtained the temperature dependence of the cell membrane permeability parameters using the grouped solute and non-ideal and non-dilute thermodynamic assumptions, and the room temperature studies with these assumptions are also limited to the two cell types, HUVECs, and H9c2 cells. Zielinski et al.[32] measured the values for b^*, B_{gg} and C_{ggg} for HUVECs at room temperature using the non-ideal thermodynamic assumptions, which are reported in Table (17). The obtained b^* value at room temperature in this work is consistent with Zielinski et al.'s reported value, but this work's obtained values for B_{gg} and C_{ggg} are different because Zielinski et al. did not investigate the responsivity of a two-degree polynomial for the grouped solute behavior, meaning $C_{ggg} = 0$. Moreover, Zielinski et al. used non-permeating solute data obtained by Ross-Rodriguez[65], which was done on HUVECs at passages beyond the supplier's recommended doubling time according to Ross-Rodriguez's laboratory notes, and Gabler Pizarro et al.[33] confirmed that based on the cell size distribution, the cells are not healthy beyond the recommended doubling time.

Table 17. Comparing the room temperature osmotic parameter values reported by Zielinski et al. [32] with those in this work.

	b^* -	B_{gg} kg water / mol	C_{ggg} (kg water / mol)^2
Zielinski et al.[32]	0.42	3.3	23.9
This work	0.425 ± 0.035	0.103 ± 0.013	0

Gabler Pizarro et al.[33] measured the five cell-type-specific parameters for HUVECs and H9c2 cells at room temperature using an iterative fitting method based on non-ideal thermodynamic assumptions, which are reported in Table (18). Gabler Pizarro et al.'s measured P_s^* value for HUVECs, and L_p^* and P_s^* values for H9c2 cells are consistent with our work's result range for those parameters, but all other parameters have different values because Gabler Pizarro et al. did not consider the C = 0 assumption, and their fitting method was limited to the kinetic cell volume data.

Table 18. Comparing the room temperature values of five cell-type-specific parameters reported by Gabler Pizarro et al. with those in this work.

		b^*	B_{gg}	C_{ggg}	L_p^*	P_s^*
		-	kg water / mol	(kg water / mol)^2	μm / atm min	μm / min
Gabler Pizarro et al.[33]	HUVECs	0.1801	0.4956	30.25	0.3434	100.8
	H9c2 cells	0.06297	0.3772	8.802	0.5869	133.4
This work	HUVECs	0.425 $\pm$ 0.035	0.103 $\pm$ 0.013	0	0.577 $\pm$ 0.089	101.92 $\pm$ 18.05
	H9c2 cells	0.449 $\pm$ 0.002	0.123 $\pm$ 0.007	0	0.584 $\pm$ 0.034	130.15 $\pm$ 6.21

The results of this work cannot be compared with the results of any previous study that used the ideal and dilute thermodynamic assumptions in their calculations. For instance, Yang et al.[66] measured the Jurkat cells' membrane permeability to water and Me_2SO, L_p and P_s, values at room temperature using a microfluidic device, and those values were 0.148 $\pm$ 0.051 μm / atm min and 3.4 $\pm$ 1.4 μm / min, respectively. However, they used the conventional two-parameter model of the cell volume, which is inherently based on the ideal thermodynamic assumptions. Therefore, our results for Jurkat cells are not comparable to those values.

In this study, we observed that the osmotically inactive fraction of the cell and the cell cytoplasm osmotic virial coefficients are temperature-dependent. The variation of inactive volume fraction with temperature has also been reported by Casula et al.[27,67] for human mesenchymal stem cells (hMSCs). These observations lead us to conclude that the cells do not act like perfect osmometers, and the cytoplasm and cell membrane complexities have a vital role in the cells' osmotic response at different temperatures and in different non-isotonic conditions. Casula et al.[27] observed the same osmotic behavior from human mesenchymal stem cells (hMSCs) and tried to model the imperfect osmotic behavior of these cells by incorporating membrane complexities such as the temporary opening of mechanosensitive channels. They explained that the cells can reach an equilibrium volume different from the initial isotonic one when isotonic conditions are re-established after contact with non-permeating or permeating solutes, and only a partial recovery of the initial isotonic volume is attained in the swelling phase.[28] They also reported that the deviation from the initial isotonic volume is more pronounced at low temperatures and decreases when the temperature increases, which is consistent with the change seen across temperatures in this work.

The cells studied in this work showed specific osmotic responses to non-isotonic conditions, which stem from their different types and biological functionalities. HUVECs, PCECs, and hCMECs are all endothelial cells but with different functionalities. Based on our results, PCECs have a relatively large permeability value to water (L_p^*) compared to the other cells at both room temperature and 0 ºC as reported in Tables (8) and (9), causing a very fast shrinkage after being in contact with the hypertonic solutions. It has been reported that corneal endothelial cells pump excess water from the corneal stroma to maintain a state of relative dehydration and prevent its tendency to swell and the cornea to lose its transparency.[68,69] Thus, the high water conductivity of corneal endothelial cells stems from their main function, the removal of stromal water. It is also

known that the corneal endothelial cells have massive permeability to other large molecules[69], which explains the PCECs' relatively higher permeability to Me_2SO than other endothelial cells. Jurkat cells, on the other hand, showed very low permeability to Me_2SO at both room temperature and 0 ºC. Jurkat cells are a type of human T lymphocytes whose primary function is controlling and shaping the body immune response using membrane receptors.[48,49] Therefore, the fact that Jurkat cells' main function is related to the protein receptors on their membrane, and they do not need to have massive permeability for large molecules, could be the reason for their low permeability to Me_2SO. H9c2 rat myoblasts, on the other hand, as a type of skeletal muscle, showed a relatively high permeability to Me_2SO at both room temperature and 0 ºC.

Using the obtained parameters in this work to model the changing cell volume and predict the cell osmotic response indicates how this work's results can help cryobiologists understand cells' cryobiological behavior and optimize cryopreservation protocols. The role of CPA concentration, loading or removal time and temperature, ice nucleation temperature, cooling rate the final temperature before plunging into liquid nitrogen, and warming rate in the cryopreservation process can all be studied using the presented non-ideal thermodynamic model. The cooling rate, determines the kinetics of water movement and whether the cells undergo large osmotic stress or a significant extent of supercooling.[15] The model can predict the intracellular water volume changes over time depending on the cooling rate, as explained in the previous chapter. The CPA addition time and temperature determine the CPA permeability and toxicity to the cells; the presented model can predict the amount of CPA entering the cells at a specific time and temperature. Inducing ice nucleation at a subzero temperature ensures enough dehydration of the cells to reduce the extent of intracellular supercooling and the probability of intracellular ice formation.[4] The amount of dehydration at various temperatures caused by inducing ice nucleation

can be investigated using the presented model. This work's model prediction for HUVECs showed logical trends for the cell volume changes during the various cryopreservation protocol. Comparing the ideal and non-ideal models showed that the ideal model overestimates the osmotic stress on the cells in the CPA addition/removal and ice nucleation steps and significantly underestimates the osmotic stress in the slow cooling process. The ideal model also predicted smaller intracellular water content than the non-ideal model and, consequently, a lower possibility of intracellular ice formation. Investigating the short CPA loading time as we kept the other conditions fixed and cooled the cells to a certain subzero temperature showed the same final conditions for the cells at that temperature. That can explain why when some cryobiologists start the cooling process shortly after adding the CPA to the cell suspension they still get acceptable cell survival. It was also demonstrated that two times larger cooling rates do not affect the cell volume noticeably but bring the cells to the final condition at the plunging temperature two times faster. Comparing the CPA removal steps conducted at room temperature and 0 ºC revealed larger osmotic stress on the cells at 0 ºC; that is why it is important for cryobiologists to keep the medium out of the refrigrator for a some time to reach the room temperature before using them for diluting the cell suspentions after thaw, otherwise the cells may die in the dilution process due to excessive osmotic stress. These obervations reveal the importance of mathematical modeling of the changing cell volume in optimizing cryopreservation protocols.

Chapter 6. Conclusion

Optimizing cryopreservation protocols by controlling the cooling rate and addition/removal steps of the CPA requires knowledge of the cells' osmotic properties. Mathematical modeling of the cell osmotic response in non-isotonic conditions by measuring the temperature dependence of the membrane permeabilities and the osmotically inactive volume of the cell is an efficient way of optimizing the cryopreservation protocols without conducting a large number of experiments. Employing non-ideal thermodynamic assumptions in the cryopreservation models can predict cell volume changes during this process. In this work, we presented a new fitting method based on both equilibrium and kinetic cell volume data to measure the five cell-type-specific parameters, b^*, B_{gg}, C_{ggg}, L_p^* and P_s^*, at room temperature and 0 ºC and model the temperature dependence of the permeability parameters, L_p^* and P_s^*, using the non-ideal thermodynamic assumptions and permeating and non-permeating solutes for five cell types, namely, human umbilical vein endothelial cells (HUVECs), H9c2 rat myoblasts, porcine corneal endothelial cells (PCECs), Jurkat cells, and human cerebral microvascular endothelial cell line (hCMEC/D3). We also investigated the possibility that the third osmotic virial coefficient, C_{ggg}, being equal to zero would result in a better fit to the experimental data for different cell types at different temperatures, which has not been investigated in previous studies. Finally, we used the obtained parameters to model the cell volume changes during a HUVEC cryopreservation protocol, demonstrated the differences between the ideal and non-ideal thermodynamic models, and investigated the impact of each step of the protocol on cell osmotic behavior.

The results of this study raise a few concerns about cells' osmotic properties. The temperature dependence of the cells' osmotically inactive fraction, b^*, and osmotic virial coefficients, B_{gg} and

C_{ggg}, suggests that understanding the cell osmotic behavior requires more and deeper investigations by accounting for the cytoplasm and membrane complexities as well as the intra- and extracellular thermodynamic conditions. The changes in the osmotically inactive fraction of the cells by changing the temperature indicate that the intracellular components are changing with temperature, which makes more sense if we consider the fact that the cells are biological entities that express different behavior in different temperatures and conditions according to their functionality. Therefore, in order to have a complete and comprehensive model for the cell osmotic response, the temperature dependence of the osmotic properties should also be modeled or at least measured at every temperature that matters in the cryopreservation protocols. However, regarding the results of this work, we can say that the 0 ºC values for the osmotic properties are the more likely ones to be relevant under cryobiological conditions. The other concern is related to the complex cell membrane behavior in the presence of a permeating CPA, especially at low temperatures, and whether it can lead to a change in the cell membrane permeability to water (L_p^*) in the presence of a permeating CPA. In this work, we used the data with the most information about a parameter to obtain that parameter to have the lowest uncertainty in our estimations: we used the non-permeating CPA cell volume data to obtain the hydraulic conductivity, L_p^*, and the permeating CPA cell volume data to obtain the permeability to CPA, P_s^*; the L_p^* obtained from the non-permeating CPA cell volume data allowed the permeating CPA cell volume data to be fit perfectly for P_s^*, meaning there is no significant extra information for L_p^* in the permeating CPA cell volume data.

References

(1) Elliott, J. A. W.; Prickett, R. C.; Elmoazzen, H. Y.; Porter, K. R.; McGann, L. E. A Multisolute Osmotic Virial Equation for Solutions of Interest in Biology. *J. Phys. Chem. B* **2007**, *111* (7), 1775–1785.

(2) Asghar, W.; El Assal, R.; Shafiee, H.; Anchan, R. M.; Demirci, U. Preserving Human Cells for Regenerative, Reproductive, and Transfusion Medicine. *Biotechnol. J.* **2014**, *9* (7), 895–903.

(3) Miyagi-Shiohira, C.; Kurima, K.; Kobayashi, N.; Saitoh, I.; Watanabe, M.; Noguchi, Y.; Matsushita, M.; Noguchi, H. Cryopreservation of Adipose-Derived Mesenchymal Stem Cells. *Cell Med.* **2015**, *8* (1–2), 3–7.

(4) Sultani, A. B.; Marquez-Curtis, L. A.; Elliott, J. A. W.; McGann, L. E. Improved Cryopreservation of Human Umbilical Vein Endothelial Cells: A Systematic Approach. *Sci. Rep.* **2016**, *6* (October), 1–14.

(5) Marquez-Curtis, L. A.; Dorobantu, L. S.; Sauvageau, D.; Elliott, J. A. W. Cryopreservation of Swine Colostrum-Derived Cells. *Cryobiology* **2020**, *97*, 168–178.

(6) Meneghel, J.; Kilbride, P.; Morris, G. J. Cryopreservation as a Key Element in the Successful Delivery of Cell-Based Therapies—A Review . *Frontiers in Medicine* . **2020**.

(7) Cottle, C.; Porter, A. P.; Lipat, A.; Turner-Lyles, C.; Nguyen, J.; Moll, G.; Chinnadurai, R. Impact of Cryopreservation and Freeze-Thawing on Therapeutic Properties of Mesenchymal Stromal/Stem Cells and Other Common Cellular Therapeutics. *Curr. Stem Cell Reports* **2022**, *8* (2), 72–92.

(8) Li, X.; Gao, D.; Ji, W. Cryopreservation of Sperm of an Endangered Species—Assamese Macaque. *Cell Preserv. Technol.* **2004**, *2* (1), 29–33.

(9) Saragusty, J.; Hildebrandt, T. B.; Behr, B.; Knieriem, A.; Kruse, J.; Hermes, R. Successful Cryopreservation of Asian Elephant (Elephas Maximus) Spermatozoa. *Anim. Reprod. Sci.* **2009**, *115* (1–4), 255–266.

(10) Salama, A.; Popova, E.; Jones, M. P.; Shukla, M. R.; Fisk, N. S.; Saxena, P. K. Cryopreservation of the Critically Endangered Golden Paintbrush (Castilleja Levisecta Greenm.): From Nature to Cryobank to Nature. *Vitr. Cell. Dev. Biol.* **2018**, *54* (1), 69–78.

(11) Saxena, A.; Bi, W.-L.; Shukla, M. R.; Cannings, S.; Bennett, B.; Saxena, P. K. Micropropagation and Cryopreservation of Yukon Draba (Draba Yukonensis), a Special Concern Plant Species Endemic to Yukon Territory, Canada. *Plants* . **2021**.

(12) Mazur, P. Kinetics of Water Loss From Cells At Subzero Temperatures and the Likelihood of Intracellular Freezing. *J. Gen. Physiol.* **1963**, *47*, 347–369.

(13) Lovelock, J. E. The Haemolysis of Human Red Blood-Cells by Freezing and Thawing. *Biochim. Biophys. Acta* **1953**, *10*, 414–426.

(14) Levitt, J. A Sulfhydryl-Disulfide Hypothesis of Frost Injury and Resistance in Plants. *J. Theor. Biol.* **1962**, *3* (3), 355–391.

(15) Mazur, P.; Leibo, S. P.; Chu, E. H. Y. A Two-Factor Hypothesis of Freezing Injury: Evidence from Chinese Hamster Tissue-Culture Cells. *Exp. Cell Res.* **1972**, *71* (2), 345–355.

(16) McGann, L. E. Differing Actions of Penetrating and Nonpenetrating Cryoprotective Agents. *Cryobiology* **1978**, *15* (4), 382–390.

(17) Lovelock, J. E. The Mechanism of the Protective Action of Glycerol against Haemolysis by Freezing and Thawing. *Biochim. Biophys. Acta* **1953**, *11* (1), 28–36.

(18) Fahy, G. M.; Lilley, T. H.; Linsdell, H.; Douglas, M. S. J.; Meryman, H. T. Cryoprotectant Toxicity and Cryoprotectant Toxicity Reduction: In Search of Molecular Mechanisms. *Cryobiology* **1990**, *27* (3), 247–268.

(19) Fahy, G. M.; Levy, D. I.; Ali, S. E. Some Emerging Principles Underlying the Physical Properties, Biological Actions, and Utility of Vitrification Solutions. *Cryobiology* **1987**, *24* (3), 196–213.

(20) Gao, D. Y.; Liu, J.; Liu, C.; McGann, L. E.; Watson, P. F.; Kleinhans, F. W.; Mazur, P.; Critser, E. S.; Critser, J. K. Andrology: Prevention of Osmotic Injury to Human Spermatozoa during Addition and Removal of Glycerol*. *Hum. Reprod.* **1995**, *10* (5), 1109–1122.

(21) Hunt, C. J.; Armitage, S. E.; Pegg, D. E. Cryopreservation of Umbilical Cord Blood: 1. Osmotically Inactive Volume, Hydraulic Conductivity and Permeability of CD34+ Cells to Dimethyl Sulphoxide. *Cryobiology* **2003**, *46* (1), 61–75.

(22) Gao, D. Y.; Chang, Q.; Liu, C.; Farris, K.; Harvey, K.; McGann, L. E.; English, D.; Jansen, J.; Critser, J. K. Fundamental Cryobiology of Human Hematopoietic Progenitor Cells I: Osmotic Characteristics and Volume Distribution. *Cryobiology* **1998**, *36* (1), 40–48.

(23) Newton, H.; Pegg, D. E.; Barrass, R.; Gosden, R. G. Osmotically Inactive Volume, Hydraulic Conductivity, and Permeability to Dimethyl Sulphoxide of Human Mature Oocytes. *J. Reprod. Fertil.* **1999**, *117* (1), 27–33.

(24) Higgins, A. Z.; Karlsson, J. O. M. Curve Fitting Approach for Measurement of Cellular Osmotic Properties by the Electrical Sensing Zone Method. I. Osmotically Inactive Volume. *Cryobiology* **2008**, *57* (3), 223–233.

(25) Higgins, A. Z.; Karlsson, J. O. M. Curve Fitting Approach for Measurement of Cellular Osmotic Properties by the Electrical Sensing Zone Method. II. Membrane Water Permeability. *Cryobiology* **2010**, *60* (2), 117–128.

(26) Vian, A. M.; Higgins, A. Z. Membrane Permeability of the Human Granulocyte to Water, Dimethyl Sulfoxide, Glycerol, Propylene Glycol and Ethylene Glycol. *Cryobiology* **2014**, *68* (1), 35–42.

(27) Casula, E.; Asuni, G. P.; Sogos, V.; Fadda, S.; Delogu, F.; Cincotti, A. Osmotic Behaviour of Human Mesenchymal Stem Cells: Implications for Cryopreservation. *PLoS One* **2017**, *12* (9), 1–21.

(28) Casula, E.; Traversari, G.; Fadda, S.; Klymenko, O. V.; Kontoravdi, C.; Cincotti, A. Modelling the Osmotic Behaviour of Human Mesenchymal Stem Cells. *Biochem. Eng. J.* **2019**, *151* (July).

(29) Prickett, R. C.; Elliott, J. A. W.; McGann, L. E. Application of the Osmotic Virial Equation in Cryobiology. *Cryobiology* **2010**, *60* (1), 30–42.

(30) McMillan, W. G.; Mayer, J. E. The Statistical Thermodynamics of Multicomponent Systems. *J. Chem. Phys.* **1945**, *13* (7), 276–305.

(31) Zielinski, M. W.; McGann, L. E.; Nychka, J. A.; Elliott, J. A. W. Nonideal Solute Chemical Potential Equation and the Validity of the Grouped Solute Approach for Intracellular Solution Thermodynamics. *J. Phys. Chem. B* **2017**, *121* (46), 10443–10456.

(32) Zielinski, M. W.; McGann, L. E.; Nychka, J. A.; Elliott, J. A. W. Measurement of Grouped Intracellular Solute Osmotic Virial Coefficients. *Cryobiology* **2020**, *97*, 198–216.

(33) Gabler Pizarro, L. A.; McGann, L. E.; Elliott, J. A. W. Permeability and Osmotic Parameters of Human Umbilical Vein Endothelial Cells and H9C2 Cells under Non-Ideal Thermodynamic Assumptions: A Novel Iterative Fitting Method. *J. Phys. Chem. B* **2021**, *125* (47), 12934–12946.

(34) L. A. Gabler Pizarro. A Novel Method of Obtaining Cell Membrane Permeability Parameters Using Non-Ideal Thermodynamic Assumptions., M.Sc. Thesis, University of Alberta, **2021**.

(35) Jaffe, E. A.; Nachman, R. L.; Becker, C. G.; Minick, C. R. Culture of Human Endothelial Cells Derived from Umbilical Veins. Identification by Morphologic and Immunologic Criteria. *J. Clin. Invest.* **1973**, *52* (11), 2745–2756.

(36) Chung, T.-W.; Liu, D.-Z.; Wang, S.-Y.; Wang, S.-S. Enhancement of the Growth of Human Endothelial Cells by Surface Roughness at Nanometer Scale. *Biomaterials* **2003**, *24* (25), 4655–4661.

(37) Huang, C.-C.; Pan, W.-Y.; Tseng, M. T.; Lin, K.-J.; Yang, Y.-P.; Tsai, H.-W.; Hwang, S.-M.; Chang, Y.; Wei, H.-J.; Sung, H.-W. Enhancement of Cell Adhesion, Retention, and Survival of HUVEC/CbMSC Aggregates That Are Transplanted in Ischemic Tissues by Concurrent Delivery of an Antioxidant for Therapeutic Angiogenesis. *Biomaterials* **2016**, *74*, 53–63.

(38) Marquez-Curtis, L. A.; Sultani, A. B.; McGann, L. E.; Elliott, J. A. W. Beyond Membrane Integrity: Assessing the Functionality of Human Umbilical Vein Endothelial Cells after Cryopreservation. *Cryobiology* **2016**, *72* (3), 183–190.

(39) Kimes, B. W.; Brandt, B. L. Properties of a Clonal Muscle Cell Line from Rat Heart. *Exp. Cell Res.* **1976**, *98* (2), 367–381.

(40) Louch, W. E.; Sheehan, K. A.; Wolska, B. M. Methods in Cardiomyocyte Isolation, Culture, and Gene Transfer. *J. Mol. Cell. Cardiol.* **2011**, *51* (3), 288–298.

(41) Tan, X.; Wang, D.; Lu, X.; Wei, H.; Zhu, R.; Zhu, S.; Jiang, H.; Yang, Z. Doxorubicin Induces Apoptosis in H9c2 Cardiomyocytes: Role of Overexpressed Eukaryotic Translation Initiation Factor 5A. *Biol. Pharm. Bull.* **2010**, *33* (10), 1666–1672.

(42) Wanka, H.; Lutze, P.; Staar, D.; Bracke, K.; Golchert, J.; Peters, J. Angiotensin Dependent and Angiotensin Independent Protective Effects of Renin-b in H9c2 Cells after Anoxia. *Sci. Rep.* **2020**, *10* (1), 19689.

(43) Hara, H.; Cooper, D. K. C. Xenotransplantation--the Future of Corneal Transplantation? *Cornea* **2011**, *30* (4), 371–378.

(44) Marquez-Curtis, L. A.; McGann, L. E.; Elliott, J. A. W. Expansion and Cryopreservation of Porcine and Human Corneal Endothelial Cells. *Cryobiology* **2017**, *77*, 1–13.

(45) Price, M. O.; Feng, M. T.; Price, F. W. J. Endothelial Keratoplasty Update 2020. *Cornea* **2021**, *40* (5), 541–547.

(46) Okumura, N.; Kinoshita, S.; Koizumi, N. Cell-Based Approach for Treatment of Corneal Endothelial Dysfunction. *Cornea* **2014**, *33 Suppl 1*, S37-41.

(47) Schneider, U.; Schwenk, H. U.; Bornkamm, G. Characterization of EBV-Genome Negative "Null" and "T" Cell Lines Derived from Children with Acute Lymphoblastic Leukemia and Leukemic Transformed Non-Hodgkin Lymphoma. *Int. J. cancer* **1977**, *19* (5), 621–626.

(48) Abraham, R. T.; Weiss, A. Jurkat T Cells and Development of the T-Cell Receptor Signalling Paradigm. *Nat. Rev. Immunol.* **2004**, *4* (4), 301–308.

(49) Wang, X.; Viswanath, R.; Zhao, J.; Tang, S.; Hewlett, I. Changes in the Level of Apoptosis-Related Proteins in Jurkat Cells Infected with HIV-1 versus HIV-2. *Mol. Cell. Biochem.* **2010**, *337* (1), 175–183.

(50) Chang, M.-C.; Wu, J.-Y.; Liao, H.-F.; Chen, Y.-J.; Kuo, C.-D. N-Farnesyloxy-Norcantharimide Inhibits Progression of Human Leukemic Jurkat T Cells through Regulation of Mitogen-Activated Protein Kinase and Interleukin-2 Production. *Anticancer. Drugs* **2015**, *26* (10), 1034–1042.

(51) Weksler, B. B.; Subileau, E. A.; Perrière, N.; Charneau, P.; Holloway, K.; Leveque, M.; Tricoire-Leignel, H.; Nicotra, A.; Bourdoulous, S.; Turowski, P.; Male, D. K.; Roux, F.; Greenwood, J.; Romero, I. A.; Couraud, P. O. Blood-Brain Barrier-Specific Properties of a Human Adult Brain Endothelial Cell Line. *FASEB J. Off. Publ. Fed. Am. Soc. Exp. Biol.* **2005**, *19* (13), 1872–1874.

(52) Tenenbaum, T.; Steinmann, U.; Friedrich, C.; Berger, J.; Schwerk, C.; Schroten, H. Culture Models to Study Leukocyte Trafficking across the Choroid Plexus. *Fluids Barriers CNS* **2013**, *10* (1), 1.

(53) Weksler, B.; Romero, I. A.; Couraud, P.-O. The HCMEC/D3 Cell Line as a Model of the Human Blood Brain Barrier. *Fluids Barriers CNS* **2013**, *10* (1), 16.

(54) Daneman, R.; Prat, A. The Blood-Brain Barrier. *Cold Spring Harb. Perspect. Biol.* **2015**, *7* (1), a020412.

(55) Marquez-Curtis, L. A.; Bokenfohr, R.; McGann, L. E.; Elliott, J. A. W. Cryopreservation of Human Cerebral Microvascular Endothelial Cells and Astrocytes in Suspension and Monolayers. *PLoS One* **2021**, *16* (4 April), e0249814.

(56) McGann, L. E.; Turner, A. R.; Turc, J.-M. Microcomputer Interface for Rapid Measurements of Average Volume Using an Electronic Particle Counter. *Med. Biol. Eng. Comput.* **1982**, *20* (1), 117–120.

(57) Prickett, R. C.; Elliott, J. A. W.; Hakda, S.; McGann, L. E. A Non-Ideal Replacement for the Boyle van't Hoff Equation. *Cryobiology* **2008**, *57* (2), 130–136.

(58) Tanaka, M.; Girard, G.; Davis, R.; Peuto, A.; Bignell, N. Recommended Table for the Density of Water between 0 C and 40 C Based on Recent Experimental Reports. *Metrologia* **2001**, *38* (4), 301–309.

(59) Physical Constants of Inorganic Compounds. in CRC Handb. Chem. Phys. (Internet Version) (Ed. Rumble, J.) (CRC Press/Taylor & Francis, 2019).

(60) Dimethyl Sulfoxide Physical Properties. Https://Www.Gaylordchemical.Com/Products/Literature/Physical-Properties/. Accessed June, 2022.

(61) Jacobs, M. H.; Stewart, D. R. A Simple Method for the Quantitative Measurement of Cell Permeability. *J. Cell. Comp. Physiol.* **1932**, *1* (1), 71–82.

(62) Zielinski, M. W.; McGann, L. E.; Nychka, J. A.; Elliott, J. A. W. Comparison of Non-Ideal Solution Theories for Multi-Solute Solutions in Cryobiology and Tabulation of Required Coefficients. *Cryobiology* **2014**, *69* (2), 305–317.

(63) Physical Constants of Organic Compounds. in CRC Handb. Chem. Phys. (Internet Version) (Ed. Rumble, J.) (CRC Press/Taylor & Francis, 2019).

(64) Values of the Gas Constant in Different Unit Systems. in CRC Handb. Chem. Phys. (Internet Version) (Ed. Rumble, J.) (CRC Press/Taylor & Francis, 2019).

(65) Ross-Rodriguez, L. U.; Elliott, J. A. W.; McGann, L. E. Non-Ideal Solution Thermodynamics of Cytoplasm. *Biopreserv. Biobank.* **2012**, *10* (5), 462–471.

(66) Yang, T.; Peng, J.; Shu, Z.; Sekar, P. K.; Li, S.; Gao, D. Determination of the Membrane Transport Properties of Jurkat Cells with a Microfluidic Device. *Micromachines* **2019**, *10* (12), 1–13.

(67) Casula, E.; Asuni, G.; Sogos, V.; Cincotti, A. HMSCs from UCB: Isolation, Characterization and Determination of Osmotic Properties for Optimal Cryopreservation. *Chem. Eng. Trans.* **2015**, *43*, 265-270 SE-Research Articles.

(68) Whikehart, D. R. Corneal Endothelium: Overview; Dartt, D. A. B. T.-E. of the E., Ed.; Academic Press: Oxford, **2010**; pp 424–434.

(69) Whiteley, H. E.; Peiffer, R. L. 38 - The Eye; HASCHEK, W. M., ROUSSEAUX, C. G., WALLIG, M. A. B. T.-H. of T. P. (Second E., Eds.; Academic Press: San Diego, **2002**; pp 539–584.

Appendix

Table A1. One room temperature equilibrium iterative process for HUVECs

5x PBS equilibrium relative volume = 0.59154, 3 molal Me_2SO equilibrium relative volume = 0.98985							
RUN	**b**	**Bgg** kg water / mol	**Cggg** (kg water / mol)^2	**Error**	**resolution**	**Bgg range**	**Cggg range**
RUN 1	0.4845	0	0	-	0.005	-	-
RUN 2	0.4845	0.115	0	0.005	0.005	0 - 10	-
RUN 3	0.4701	0.115	0	-	0.005	-	-
RUN 4	**0.4701**	**0.115**	**0**	**0.005**	**0.005**	**0 - 10**	**-**

Table A2. One 0 ºC equilibrium iterative process for HUVECs

5x PBS equilibrium relative volume = 0.5448, 3 molal Me_2SO equilibrium relative volume = 0.7							
RUN	**b**	**Bgg** kg water / mol	**Cggg** (kg water / mol)^2	**Error**	**resolution**	**Bgg range**	**Cggg range**
RUN 1	0.4291	0	0	-	0.005	-	-
RUN 2	0.4291	1.95	19.15	0.0005	0.005	0 - 5	0 - 40
RUN 3	0.1685	1.96	20.15	-	0.005	-	-
RUN 4	0.1685	1	15.25	0.0007	0.005	0 - 5	0 - 40
RUN 5	0.1728	1	15.25	-	0.005	-	-
RUN 6	0.1728	1.2	22.95	0.0007	0.005	0 - 5	0 - 40
RUN 7	0.1487	1.2	22.95	-	0.005	-	-
RUN 8	0.1487	1.15	22	0.0007	0.005	0 - 5	0 - 40
RUN 9	0.1508	1.15	22	-	0.005	-	-
RUN 10	0.1508	1.15	22.3	0.0007	0.005	0 - 5	0 - 40
RUN 11	0.15	1.15	22.3	-	0.005	-	-
RUN 12	0.15	1.15	22.35	0.0007	0.005	0 - 5	0 - 40
RUN 13	**0.1498**	**1.15**	**22.35**	**-**	**0.005**	-	-

Table A3. One room temperature equilibrium iterative process for Jurkat cells

5x PBS equilibrium relative volume = 0.5741, 3 molal Me_2SO equilibrium relative volume = 0.8708							
RUN	**b**	**Bgg** kg water / mol	**Cggg** (kg water / mol)^2	**Error**	**resolution**	**Bgg range**	**Cggg range**
RUN 1	0.4617	0	0	-	0.05	-	-
RUN 2	0.4617	0.8	21.5	0.00007	0.05	0 - 5	5 - 40
RUN 3	0.1905	0.8	21.5	-	0.05	-	-
RUN 4	0.1905	0.65	23.65	0.00003	0.05	0 - 5	5 - 40
RUN 5	0.1827	0.65	23.65	-	0.05	-	-
RUN 6	0.1827	0.65	23.89	0.00007	0.05	0 - 3	5 - 40
RUN 7	**0.1821**	**0.65**	**23.89**	**-**	**0.05**	**-**	**-**

Table A4. One 0 ºC equilibrium iterative process for Jurkat cells

5x PBS equilibrium relative volume = 0.5444, 3 molal Me_2SO equilibrium relative volume = 0.7401							
RUN	**b**	**Bgg** kg water / mol	**Cggg** (kg water / mol)^2	**Error**	**resolution**	**Bgg range**	**Cggg range**
RUN 1	0.4246	0	0		0.05	-	-
RUN 2	0.4246	1.25	21.2	0.00007	0.05	0 - 5	5 - 40
RUN 3	0.1424	1.25	21.2		0.05	-	-
RUN 4	0.1424	0.9	24.6	0.00003	0.05	0 - 5	5 - 40
RUN 5	0.1282	0.9	24.6		0.05	-	-
RUN 6	0.1282	0.9	25.35	0.00007	0.05	0 - 3	5 - 40
RUN 7	0.1263	0.9	25.35		0.05	-	-
RUN 8	0.1263	0.9	25.45	0.0002	0.05	0 - 3	5 - 40
RUN 9	0.126	0.9	25.45		0.05	-	-
RUN 10	**0.126**	**0.9**	**25.45**	**0.0003**	**0.05**	**0 - 3**	**5 - 40**

Table A5. One room temperature equilibrium iterative process for PCECs

5x PBS equilibrium relative volume = 0.59, 3 molal Me_2SO equilibrium relative volume = 1.06							
RUN	**b**	**Bgg** kg water / mol	**Cggg** (kg water / mol)^2	**Error**	**resolution**	**Bgg range**	**Cggg range**
RUN 1	0.4823	0	0	-	0.005	-	-
RUN 2	0.4823	0.07	0	0.005	0.005	0 - 10	-
RUN 3	0.4730	0.07	0	-	0.005	-	-
RUN 4	0.4730	0.075	0	0.005	0.005	0 - 10	-
RUN 5	**0.4724**	**0.075**	**0**	**-**	**0.005**	**-**	**-**

Table A6. One 0 ºC equilibrium iterative process for PCECs

5x PBS equilibrium relative volume = 0.557, 3 molal Me_2SO equilibrium relative volume = 0.807							
RUN	**b**	**Bgg** kg water / mol	**Cggg** (kg water / mol)^2	**Error**	**resolution**	**Bgg range**	**Cggg range**
RUN 1	0.4413	0	0		0.05	-	-
RUN 2	0.4413	1.1	20.85	0.00003	0.05	0 - 5	5 - 40
RUN 3	0.1673	1.1	20.85		0.05	-	-
RUN 4	0.1673	0.8	22.4	0.00005	0.05	0 - 5	5 - 40
RUN 5	0.1594	0.8	22.4		0.05	-	-
RUN 6	0.1594	0.85	26.35	0.00007	0.05	0 - 3	5 - 40
RUN 7	0.1499	0.85	26.35		0.05	-	-
RUN 8	0.1499	0.85	26.85	0.00003	0.05	0 - 3	5 - 40
RUN 9	**0.1487**	**0.85**	**26.85**		**0.05**	**-**	**-**

Table A7. One room temperature equilibrium iterative process for hCMECs

5x PBS equilibrium relative volume = 0.5711, 3 molal Me_2SO equilibrium relative volume = 0.987							
RUN	**b**	**Bgg** kg water / mol	**Cggg** (kg water / mol)^2	**Error**	**resolution**	**Bgg range**	**Cggg range**
RUN 1	0.4608	0	0	-	0.05	-	-
RUN 2	0.4608	0.45	23.4	0.00007	0.05	0 - 5	5 - 40
RUN 3	0.1827	0.45	23.4	-	0.05	-	-
RUN 4	0.1827	0.45	26.4	0.00003	0.05	0 - 5	5 - 40
RUN 5	0.1756	0.45	26.4	-	0.05	-	-
RUN 6	**0.1756**	**0.45**	**26.45**	**0.00007**	**0.05**	**0 - 3**	**5 - 40**

Table A8. One 0 ºC equilibrium iterative process for hCMECs

5x PBS equilibrium relative volume = 0.512, 3 molal Me_2SO equilibrium relative volume = 0.6793							
RUN	**b**	**Bgg** kg water / mol	**Cggg** (kg water / mol)^2	**Error**	**resolution**	**Bgg range**	**Cggg range**
RUN 1	0.3865	0	0	-	0.05	-	-
RUN 2	0.3865	2	20.35	0.00001	0.05	0 - 5	5 - 40
RUN 3	0.0999	2	20.35	-	0.05	-	-
RUN 4	0.0999	1.35	23.64	0.0001	0.05	0 - 5	5 - 40
RUN 5	0.0820	1.35	23.64	-	0.05	-	-
RUN 6	0.0820	1.15	22.55	0.0001	0.05	0 - 3	5 - 40
RUN 7	0.0827	1.15	22.55	-	0.05	-	-
RUN 8	0.0827	1.15	22.5	0.0001	0.05	0 - 3	5 - 40
RUN 9	0.0828	1.15	22.5	-	0.05	-	-
RUN 10	**0.0828**	**1.15**	**22.5**	**0.0001**	**0.05**	**0 - 3**	**5 - 40**

Table A9. One room temperature equilibrium iterative process for H9c2 cells

5x PBS equilibrium relative volume = 0.5744, 3 molal Me_2SO equilibrium relative volume = 0.988							
RUN	**b**	**Bgg** kg water / mol	**Cggg** (kg water / mol)^2	**Error**	**resolution**	**Bgg range**	**Cggg range**
RUN 1	0.4639	0	0	-	0.005	-	-
RUN 2	0.4639	0.115	0	0.005	0.005	0 - 10	-
RUN 3	0.4491	0.115	0	-	0.005	-	-
RUN 4	0.4491	0.115	0	0.005	0.005	0 - 10	-
RUN 5	**0.4491**	**0.115**	**0**	**-**	**0.005**	**-**	**-**

Table A10. First 0 ºC equilibrium iterative process for H9c2 cells

5x PBS equilibrium relative volume = 0.4764, 3 molal Me_2SO equilibrium relative volume = 0.7129							
RUN	**b**	**Bgg** kg water / mol	**Cggg** (kg water / mol)^2	**Error**	**resolution**	**Bgg range**	**Cggg range**
RUN 1	0.3403	0	0		0.05	-	-
RUN 2	0.0217	0.9	18.95	0.00003	0.05	0 - 5	5 - 40
RUN 3	0.0217	0.95	20.8		0.05	-	-
RUN 4	0.0154	0.95	20.8	0.00005	0.05	0 - 5	5 - 40
RUN 5	0.0154	0.95	21.1		0.05	-	-
RUN 6	0.0144	0.95	21.1	0.00007	0.05	0 - 3	5 - 40
RUN 7	0.0144	0.95	21.15		0.05	-	-
RUN 8	0.0142	0.95	21.15	0.00003	0.05	0 - 3	5 - 40
RUN 9	**0.0142**	**0.95**	**21.15**		**0.05**	**-**	**-**

Table A11. Second 0 ºC equilibrium iterative process for H9c2 cells

5x PBS equilibrium relative volume = 0.4875, 3 molal Me_2SO equilibrium relative volume = 0.7323							
RUN	**b**	**Bgg** kg water / mol	**Cggg** (kg water / mol)^2	**Error**	**resolution**	**Bgg range**	**Cggg range**
RUN 1	0.3543	0	0	-	0.05	-	-
RUN 2	0.3543	1.5	24.6	0.00003	0.05	0 - 5	5 - 40
RUN 3	0.0316	1.5	24.6	-	0.05	-	-
RUN 4	0.0316	0.95	23.55	0.00005	0.05	0 - 5	5 - 40
RUN 5	0.0273	0.95	23.55	-	0.05	-	-
RUN 6	0.0273	0.95	23.75	0.0001	0.05	0 - 3	5 - 40
RUN 7	0.0266	0.95	23.75	-	0.05	-	-
RUN 8	0.0266	0.95	23.8	0.00003	0.05	0 - 3	5 - 40
RUN 9	**0.0265**	**0.95**	**23.8**	**-**	**0.05**	**-**	**-**

Table A12. Third 0 ºC equilibrium iterative process for H9c2 cells

5x PBS equilibrium relative volume = 0.4875, 3 molal Me_2SO equilibrium relative volume = 0.7129							
RUN	**b**	**Bgg** kg water / mol	**Cggg** (kg water / mol)^2	**Error**	**resolution**	**Bgg range**	**Cggg range**
RUN 1	0.3543	0	0	-	0.05	-	-
RUN 2	0.3543	1.65	24.2	0.00003	0.05	0 - 5	5 - 40
RUN 3	0.0347	1.65	24.2	-	0.05	-	-
RUN 4	0.0347	1	22.85	0.0001	0.05	0 - 5	5 - 40
RUN 5	0.0302	1	22.85	-	0.05	-	-
RUN 6	0.0302	1	23.05	0.0003	0.05	0 - 3	5 - 40
RUN 7	0.0295	1	23.05	-	0.05	-	-
RUN 8	0.0295	1	23.1	0.0003	0.05	0 - 3	5 - 40
RUN 9	**0.0294**	**1**	**23.1**	**-**	**0.05**	**-**	**-**

Table A13. Fourth 0 ºC equilibrium iterative process for H9c2 cells

5x PBS equilibrium relative volume = 0.4875, 3 molal Me_2SO equilibrium relative volume = 0.6889							
RUN	**b**	**Bgg** kg water / mol	**Cggg** (kg water / mol)^2	**Error**	**resolution**	**Bgg range**	**Cggg range**
RUN 1	0.3543	0	0	-	0.05	-	-
RUN 2	0.3543	1.9	24.7	0.00003	0.05	0 - 5	5 - 40
RUN 3	0.0362	1.9	24.7	-	0.05	-	-
RUN 4	0.0362	1.1	23.75	0.00005	0.05	0 - 5	5 - 40
RUN 5	0.0288	1.1	23.75	-	0.05	-	-
RUN 6	0.0288	1.1	24.2	0.00007	0.05	0 - 3	5 - 40
RUN 7	0.0274	1.1	24.2	-	0.05	-	-
RUN 8	0.0274	1.1	24.25	0.00003	0.05	0 - 3	5 - 40
RUN 9	**0.0273**	**1.1**	**24.25**	**-**	**0.05**	**-**	**-**

Table A14. Fifth 0 ºC equilibrium iterative process for H9c2 cells

5x PBS equilibrium relative volume = 0.4764, 3 molal Me_2SO equilibrium relative volume = 0.6889							
RUN	**b**	**Bgg** kg water / mol	**Cggg** (kg water / mol)^2	**Error**	**resolution**	**Bgg range**	**Cggg range**
RUN 1	0.3403	0	0	-	0.05	-	-
RUN 2	0.3403	1.8	23.75	0.00003	0.05	0 - 5	5 - 40
RUN 3	0.0171	1.8	23.75	-	0.05	-	-
RUN 4	0.0171	1.05	22.3	0.0001	0.05	0 - 5	5 - 40
RUN 5	0.0117	1.05	22.3	-	0.05	-	-
RUN 6	0.0117	1.05	22.55	0.0003	0.05	0 - 3	5 - 40
RUN 7	0.0109	1.05	22.55	-	0.05	-	-
RUN 8	0.0109	1.05	22.6	0.0003	0.05	0 - 3	5 - 40
RUN 9	**0.0107**	**1.05**	**22.6**	**-**	**0.05**	**-**	**-**

Table A15. Sixth 0 ºC equilibrium iterative process for H9c2 cells

5x PBS equilibrium relative volume = 0.4727, 3 molal Me_2SO equilibrium relative volume = 0.7129							
RUN	**b**	**Bgg** kg water / mol	**Cggg** (kg water / mol)^2	**Error**	**resolution**	**Bgg range**	**Cggg range**
RUN 1	0.3356	0	0	-	0.05	-	-
RUN 2	0.3356	1.6	24.2	0.00003	0.05	0 - 5	5 - 40
RUN 3	0.0038	1.6	24.2	-	0.05	-	-
RUN 4	0.0038	1	22.85	0.00009	0.05	0 - 5	5 - 40
RUN 5	0..0042	1	22.85	-	0.05	-	-
RUN 6	0..0043	1	22.9	0.00007	0.05	0 - 3	5 - 40
RUN 7	0.0048	1	22.9	-	0.05	-	-
RUN 8	0.0048	1	23.1	0.00003	0.05	0 - 3	5 - 40
RUN 9	**0.0048**	**1**	**23.1**	**-**	**0.05**	**-**	**-**

Table A16. Seventh 0 ºC equilibrium iterative process for H9c2 cells

5x PBS equilibrium relative volume = 0.4727, 3 molal Me_2SO equilibrium relative volume = 0.7323							
RUN	**b**	**Bgg** kg water / mol	**Cggg** (kg water / mol)^2	**Error**	**resolution**	**Bgg range**	**Cggg range**
RUN 1	0.3356	0	0	-	0.05	-	-
RUN 2	0.3356	1.45	24.85	0.00003	0.05	0 - 5	5 - 40
RUN 3	0.0022	1.45	24.85	-	0.05	-	-
RUN 4	0.0022	0.9	22	0.00009	0.05	0 - 5	5 - 40
RUN 5	0.0035	0.9	22	-	0.05	-	-
RUN 6	0.0035	0.9	21.9	0.00007	0.05	0 - 3	5 - 40
RUN 7	0.0038	0.9	21.9	-	0.05	-	-
RUN 8	0.0038	0.9	21.9	0.00003	0.05	0 - 3	5 - 40
RUN 9	**0.0038**	**0.9**	**21.9**	**-**	**0.05**	**-**	**-**